AD_____

Award Number: W81XWH-12-1-0366

TITLE: Integrated Immunotherapy for Breast Cancer

PRINCIPAL INVESTIGATOR: Peter P. Lee, MD

CONTRACTING ORGANIZATION:
Beckman Research Institute of City of Hope
Duarte, CA 91010

REPORT DATE: September 2016

TYPE OF REPORT: Annual

PREPARED FOR: U.S. Army Medical Research and Materiel Command
Fort Detrick, Maryland 21702-5012

REPORT DOCUMENTATION PAGE

Form Approved
OMB No. 0704-0188

1. REPORT DATE	**2. REPORT TYPE**	**3. DATES COVERED**
September 2016	Annual	1 Sep 2015 - 31 Aug 2016

4. TITLE AND SUBTITLE

Integrated Immunotherapy for Breast Cancer

5a. CONTRACT NUMBER

5b. GRANT NUMBER
W81XWH-12-1-0366

5c. PROGRAM ELEMENT NUMBER

6. AUTHOR(S)

Peter P. Lee, MD

E-Mail: plee@coh.org

5d. PROJECT NUMBER

5e. TASK NUMBER

5f. WORK UNIT NUMBER

7. PERFORMING ORGANIZATION NAME(S) AND ADDRESS(ES)

Beckman Research Institute of City of Hope
Dept. of Cancer Immunotherapeutics and Tumor Immunology (CITI)
1500 East Duarte Rd.
Duarte, CA 91010

8. PERFORMING ORGANIZATION REPORT NUMBER

9. SPONSORING / MONITORING AGENCY NAME(S) AND ADDRESS(ES)
U.S. Army Medical Research and Materiel Command
Fort Detrick, Maryland 21702-5012

10. SPONSOR/MONITOR'S ACRONYM(S)

11. SPONSOR/MONITOR'S REPORT NUMBER(S)

12. DISTRIBUTION / AVAILABILITY STATEMENT
Approved for Public Release; Distribution Unlimited

13. SUPPLEMENTARY NOTES

14. ABSTRACT
Over the last 12 months of this award, we have focused on developing an in-depth understanding of the immune system in the setting of the tumor microenvironment. We have made progress in developing methods to better analyze the relationships between primary tumor and metastatic growths with their surrounding microenvironments, and implications for immune response and dendritic cell function *in vitro* using 3D microculture techniques. We have further investigated and tested alternative methods for tumor eradication using combinatorial drugs in attempts to restore/enhance the immune response. Additionally, we continue preparing breast cancer cell lines to aid quantifying progress in *in vivo* studies using mouse models. We anticipate that the progress made in these last 12 months will lead to combining observations into *in vitro* and *in vivo* models to better test our combinatorial immunotherapeutic strategies, restore dendritic cell function in cancer, and identifying novel tumor-associated stroma targets.

15. SUBJECT TERMS
Breast Cancer, immunotherapy, tumor microenvironment, dendritic cells, metastasis, cancer stroma.

16. SECURITY CLASSIFICATION OF:			**17. LIMITATION OF ABSTRACT**	**18. NUMBER OF PAGES**	**19a. NAME OF RESPONSIBLE PERSON**
a. REPORT	**b. ABSTRACT**	**c. THIS PAGE**			**19b. TELEPHONE NUMBER** *(include area code)*
U	U	U	UU		

Table of Contents

Page

INTRODUCTION:

The immune system and cancer are both complex biological systems that interact and affect each other. While there have been recent successes in cancer immunotherapy including PROVENGE, a dendritic cell based vaccine for prostate cancer, and antibodies blocking immune checkpoints (CTLA-4 and PD-1) for melanoma/lung cancer, these have produced clinical benefits only in a subset of patients. The intimate relationships between cancer cells, immune cells, and tumor associated stromal cells must be explored and investigated in order to truly have an effective immunotherapy for breast cancer. It has more recently become clear that not only does the immune system respond to cancer cells, but the process goes both ways, with cancer also able to suppress the host immune system. Tumor-infiltrating lymphocytes (TILs) have been shown to be functionally impaired in many cancers (*2*). In tumors where TILs were found to be functional, the prognosis was consistently favorable (*3, 4*). The collective data suggest that T cell infiltration—when functionally active—leads to a favorable outcome in breast cancer. These data concerning the tumor microenvironment complement our own findings that changes in immune cells within tumor-draining lymph nodes (TDLNs) strongly correlate with clinical outcome in breast cancer (*5*). Despite the complexity, certain elements can be teased out and focused upon for maximal impact. Our previous studies have led to key insights into the mechanisms behind the immune dysfunction that breast cancer causes. Comprehending how the different phases—activation, expansion and effector functions—of a normally functioning immune response are disrupted in the presence of breast cancer will allow us to develop strategies to counteract the problems and restore immune function to optimal levels in patients. This focus on unraveling the dynamics between breast cancer and host immune system in a comprehensive and systematic manner is the underlying principle of my goal to develop rational combination immunotherapy for breast cancer, one that is truly effective long term at eliminating metastases and thereby preventing relapse in breast cancer patients. In order to build on the observations my lab has made with regards to cancer-dendritic cell function and immune cell-cancer relationships, immune responses within the tumor microenvironment must be analyzed in depth to identify unique markers, molecular and cytokine signals, and associated cell populations which may be aiding in immunosuppression. To this end, I have built a strong research team for this project, which includes assistant research professor Dr. Brile Chung, staff scientist Dr. Young Min Chung, PhD postdoctoral fellow Dr. Manasi Kamat, and research associate Gilbert Acosta. We worked closely with clinical collaborators at the City of Hope under an IRB approved protocol. In this annual report, I will discuss the foundation being laid toward the goals outlined in our statement of work, and the approaches that we will test to remedy the global immune dysfunction in breast cancer.

BODY:

We have a strong research team for this project, which includes assistant research professor Dr. Brile Chung, staff scientist Dr. Young Min Chung, PhD postdoctoral fellow Dr. Manasi Kamat, and research associate Gilbert Acosta. We worked closely with the CoH IRB office on a human subject's protocol which has been approved. We have close collaborations with breast cancer surgeons, pathologists, and the tissue bank at CoH in order to procure breast cancer tissue, lymph node, and blood samples for our analyses. Animal work has begun under two animal protocols (IUCAC #13042 and #14040) which have been approved at City of Hope and the DoD. Our team has been working hard on establishing cell lines, protocols, *in vitro* and *in vivo* experiments to build a solid foundation and direction for progressing towards the tasks in our statement of work. Listed below are the main aims which we proposed, corresponding tasks from our statement of work, and our progress to-date.

Task 1. Investigate mechanisms by which stromal cells modulate and support breast cancer cells within the tumor microenvironment and develop therapeutic strategies to target stromal cells: months 1-60.

1a. Identify genes/splice variants and pathways in stromal cells from primary and metastatic breast tumors that are involved in modulating/attracting cancer cells within the 3D tumor microenvironment (month 1-60).

1b. Identify unique growth factors, cytokines, or chemokines that promote breast cancer cell proliferation (month 1-60).

1c. Identify stromal factors with primary/metastatic breast tumors that suppress immune cell function (month 1-60).

1d. develop therapeutic strategies to modulate/target breast cancer stromal cells (month 12-60).

Task 2. Investigate mechanisms by which chronic IL6 affects immune function: months 1-36.

2a. Gene expression analyses and flow cytometry to measure expression of positive and negative signaling regulators (month 1-60).

2b. T cell polarization and functional assays (month 1-60).

Task 3. Select Optimal Integrated Immunotherapy Combinations in Animal Models for Clinical Development: months 12-60.

3a. Optimize post-surgical murine model of breast cancer metastasis (month 12-36).

3b. DC vaccination optimization by restoration of DC clustering and maturation (months 24-48).

3c. Optimization of the amplification and effector phases by correcting chronic IL6-mediated defective T cell responses (month 24-48).

3d. Combining optimal DC vaccination strategies with cytokine signaling modulation therapeutics for optimal immunotherapeutic regimens (month 36-60).

3e. Testing other strategies and combinations. (month 48-60).

Results:

Task 1. Investigate mechanisms by which stromal cells modulate and support breast cancer cells within the tumor microenvironment and develop therapeutic strategies to target stromal cells: months 1-60.

1a. Identify genes/splice variants and pathways in stromal cells from primary and metastatic breast tumors that are involved in modulating/attracting cancer cells within the 3D tumor microenvironment (month 1-60).

1b. Identify unique growth factors, cytokines, or chemokines that promote breast cancer cell proliferation (month 1-60).

1c. Identify stromal factors with primary/metastatic breast tumors that suppress immune cell function (month 1-60).

1d. develop therapeutic strategies to modulate/target breast cancer stromal cells (month 12-60).

In order to gain knowledge on the molecules and factors which stromal cells modulate and support breast cancer cells in the tumor microenvironment, we need to establish a better understanding of the dynamics between immune cells and the tumor microenvironment. To this end, we have worked to establish an *in vitro/ex vivo* model which helps mimic cell-cell interactions in a 3D microenvironment. It has been established in recent years that 3D cell culture environments provide a more physiological representation of cell interactions. 3D cultures also produce markers and behavior that might not be seen on traditional monolayer culture experiments, and applies also specifically to the breast cancer setting (*6*). The tumor microenvironment is comprised of heterogeneous populations of cells including cancer, immune, and cancer-associated stromal cells (*7*). Clinical data and experimental models have shown that the extent and nature of immune infiltrations into tumors is an important independent prognostic factor (*8*). Recent findings suggest that cancer associated stroma (CAS) (*7*) is another important regulator of tumor growth and progression which may also modulate the recruitment, activation status, and retention of immune cells within the tumor microenvironment (*9*). Therefore, targeting the CAS plus cancer cells is essential for the success of cancer immunotherapy.

Progression of tumor growth and initiation of metastasis is critically dependent on the reciprocal interactions between cancer cells and tumor associated stroma. CAS have been known to promote inhibitory effect on T cells by producing various factors and cytokines such as TGF beta, VEGF, HGF, IL-6, and IL-17 (*10*).

Human brain metastatic stroma recruits breast cancer cells via chemokines CXCL16 and CXCL12

Brain metastasis is the most lethal outcome of breast cancer, leading to death within 4-6 months in 10-15% of patients once detected (*11, 12*). For brain metastasis to occur, cancer cells from the primary tumor must migrate to the brain, traverse the blood-brain barrier (BBB), and proliferate within the brain parenchyma (*13*). Emerging data suggest that the outcome of metastasis is influenced by the specific organ microenvironment stromal cells that permit the effective colonization and growth of circulating tumor cells (*14*). We hypothesized that mesenchyme-derived fibroblasts, the major cell population of tumor stroma, promote invasion, survival, and proliferation of migrating cancer cells to facilitate breast cancer brain metastasis.

Conventional methods to model the metastatic process ex vivo mainly involve two dimensional (2D) monolayer in vitro systems, which do not recapitulate the 3D in vivo microenvironment. Cell-cell and cell-extracellular matrix (ECM) interactions in 3D spatial environment are critical for understanding the complex cross-talk mechanisms between cancer and stromal cells. For example, both gene and protein expressions in an ex vivo 3D culture system appear to conserve various paracrine-dependent cellular interactions that occur in vivo microenvironment (*15-17*). Furthermore, studies have shown that testing of chemotherapy treatments or immunotherapies based on 2D monolayer systems does not correspond with results in an in vivo setting, further demonstrating the limitations of 2D monolayer systems (*18*). Hence, developing and testing the effectiveness of cancer therapies for breast cancer in vitro require recreation of the 3D breast cancer microenvironment composed of stroma and cancer cells derived from the same patient as one functional unit.

Cancer-associated fibroblasts (CAFs) have been shown to produce various chemokines to facilitate angiogenesis and cancer cell migration (*19*). To investigate the role of CAFs in breast cancer brain metastasis, we isolated and expanded fibroblasts derived from normal breast, primary and brain metastatic tumor tissues. Utilizing 3-D ex-vivo aggregates composed of different CAFs with cancer cells, we evaluated the expression of various chemokines and growth factors by RNA-Seq, real-time quantitative RT-PCR, immunohistochemical staining, and ELISA. These studies showed that metastatic CAFs from brain metastases produce high levels of chemokines CXCL12 and CXCL16, promoting the recruitment of patient-specific breast cancer cells in a 3-D aggregate system. Moreover, blocking of CXCR4, the chemokine receptor for CXCL12, and neutralization of CXCL16, the ligand for CXCR6 in patient-specific cancer cells significantly prevented the migration of cancer cells to the tumor microenvironment. These novel findings within our 3D CAF aggregate system provide a

proof of principle that applying a combination therapy of chemokine binding modulation may provide an effective therapeutic strategy to prevent tumor progression and metastasis.

Isolation of breast cancer cells and CAFs from patient tumor tissues

To observe the role of CAFs derived from breast tumors, we received fresh human breast tumor tissues from patients following biopsy. We divided the tumor samples according to their tumor stage and patient status (Table 1). For normal control, the tissues were obtained from either contralateral side of breast cancer patients, or the samples from the patients treated with prophylactic mastectomy. IHC analysis of both human primary breast and brain metastatic tumor samples showed the presence of Vimentin positive stromal cells surrounding epithelial-specific Cytokeratin-positive breast cancer cells (Figure 1A). To study these cells and develop an ex-vivo culture system that allows expansion of both patient-specific breast cancer cells and CAFs, human breast tumor tissues were mechanically dissociated into small fragments and plated onto tissue culture plate in medium supplemented with epidermal and keratinocyte growth factor. Within 2 weeks, both non-adherent CD326+ cancer cells and monolayers of adherent CD326-CD44+ cells expanded by outgrowth from the initial adherent tumor fragments. To investigate whether CD326-CD44+ adherent cells express mesenchyme-derived surface markers, we performed immunophenotypic characterization of the monolayer generated in breast tumor fragment cultures after 3 weeks by flow cytometry. Nearly all the ex vivo expanded mesoderm-derived fibroblasts from normal breast and CAFs from primary and brain metastatic tumors expressed the common mesenchyme markersCD44, CD90, CD105, CD166, and CD140β (Figure 1B). In contrast, CD326+ patient-derived breast cancer cells did not display the surface markers expressed by CAFs (Figure 1C).

Both semi-quantitative and quantitative PCR analysis demonstrated that EGF, FGF, and IGF-1 (factors known to support growth of cancer cells) are expressed by both primary tumor and brain metastasis CAFs (Figure 1D). This provides evidence that cultured CAFs produce factors important for maintenance of patient specific breast cancer cells. Since bone marrow-derived mesenchymal stem cells (MSCs) are known to reside within breast tumor microenvironment and express similar surface markers as CAFs, trans-differentiation assays were performed to determine if some of the CAF populations were capable of undergoing adipogenesis as observed in MSCs. In addition, we further investigated the expression of STRO-1, the surface antigen known to express by bone marrow MSCs. Our data showed that CAFs derived from primary breast tumor and brain metastasis express higher levels of STRO-1 and can differentiate into adipocytes, suggesting our CAF culture contains MSC like cell populations (Figure 1E) (*20, 21*).

Generation of human breast tumor-derived CAF aggregates

2-D culture models do not fully replicate complexities in tumor tissues, such as multidimensional cellular structure, extracellular matrixes, and divergent gene expression patterns (*22*). Hence, we generated 3-D aggregates from cells cultured out of normal breast tissue, primary tumors and metastasis to recapitulate similar cellular complexities displayed by the human tumor microenvironment. Normal breast mesenchyme and patient-specific CAF aggregates were created by centrifugation of monolayers generated from the tissue culture, followed by further culturing on nucleo-pore filters (Figure 2A). Histologic analysis of CAF aggregates at day 5 (post-culture) showed the morphological similarities, when compared to patient tissue samples (data not shown). In order to demonstrate the ability of 3-D aggregates to produce and maintain ECM and CAF markers, cell aggregates were cultured for 2 weeks and paraffin-sectioned for IHC analyses. Histologic analysis of the paraffin aggregates illustrated that important ECM components such as Collagen IV and Fibronectin were preserved in all the aggregates when compared to fresh human breast tumor tissues (Figure 2B). Expression of Fibroblastic Activating Protein (FAP) and alpha Smooth Muscle Actin (α-SMA) has been well described in myofibroblasts and CAF (*23-25*). As expected, both FAP and α-SMA alpha smooth muscle actin expressing cells were more prevalent in the primary and brain metastasis aggregates when compared to the normal fibroblast aggregates (Figure 2B). To further investigate whether FAP+ α-SMA+ cells detected from brain metastasis aggregates were originated from cell types of the central nervous system (CNS), such as astrocytes and ependymal cells, we examined the expression of glilal fibrillary acidic protein (GFAP) in brain metastasis aggregates (data not shown). The data showed that CAFs from brain metastasis do not express GFAP, suggesting that they are of non-CNS origin (*26*).

To demonstrate whether our CAF aggregate system can maintain and promote proliferation of cancer cells, we generated CAF aggregates mixed with patient-derived breast cancer cells and measured Ki-67 expression in cancer cells. Here, we included patient-specific cancer cells into our patient-derived CAF aggregate culture system in order to mimic more natural tumor microenvironment setting. Data shown in Figure 2C demonstrate that our 3D co-culture system supports proliferation of patient-derived cancer cells. We detected significantly higher numbers of Ki-67 positive cancer cells in primary and metastatic CAF aggregates than from normal breast fibroblasts aggregates (Figure 2C). Since the genes for mesenchyme-derived growth factors known to promote cancer cell proliferation are well expressed in CAF populations (Figure 1D) the data provide evidence that these aggregates are functional. Overall, these results showed that the *ex vivo* CAF 3-D aggregates system served as a sufficient ECM producing microenvironment and provided growth factors capable of maintaining CAF characteristics.

mRNA level expression and histological analysis of chemokines in primary tumor and brain metastasis derived human breast CAF 3-D aggregates To investigate whether CAF aggregates generated from primary or metastatic breast tumor tissues display different gene expression patterns, RNA samples were extracted from each independent aggregate culture and analyzed via RNA-Seq. The raw FASTQ files obtained from RNA-seq were analyzed via CLC Genomic Workbench to compare gene expression levels between sample groups. Differences in relative gene expression levels between each aggregate group (normal, primary tumor, and brain metastasis) are illustrated as a heat map (Figure 3A) generated through hierarchical clustering. Additionally, the lists of the top differentially expressed growth factors and cytokines are shown in Table 2**.** Based on gene transcript expression differences, among the consistently over expressed transcripts in the metastatic aggregates are CXCL16, CXCL12, and platelet derived growth factor alpha (PDGFA). Moreover, the fold change of the gene expression of chemokine CXCL16 in the metastatic samples compared to the normal and primary samples (5.34 and 6.436) is significantly higher respectively. While reports have shown that tumors produce high levels of chemokines including CXCL12, these studies did not identify CAFs as the source within the tumor microenvironment (*27, 28*). High-level secretion of CXCL16 from patient-derived brain metastasis CAFs has not been reported. To further validate differentially expressed transcripts from each group of aggregate, quantitative RT-PCR analyses (Figure 3B) and IHC were performed on patient tissues and CAF aggregates (Figure 3C). Relative changes in chemokine genes expression and proteins levels were directly related to the RNA-seq and qRT-PCR data illustrated in Figure 3A and B. While CXCL16 can exist as either secreted or trans-membrane bound forms, only the soluble form is known to function as a chemotactic ligand for CXCR6 expressing cancer and immune cells (*29-31*). Production of the secreted form of CXCL16 was analyzed via ELISA from each representative CAF population (Figure 3D). High levels of secreted chemokines observed in the ELISA assay from brain metastatic CAF aggregates provides a mechanism by which breast cancer cells are recruited to the metastatic brain microenvironment.

Effects of cancer associated fibroblasts in migration of cancer cells

Based on our studies indicating that brain metastatic CAF aggregates produced higher levels of chemokines CXCL12 and CXCL16 as compared to normal breast fibroblasts or primary tumor CAF aggregates, we performed cancer cell migration assays (using MCF-Her2 cells or patient-specific cancer cells) to investigate the relative propensity of breast cancer cells to migrate to these different microenvironments. To demonstrate whether high levels of CXCL12 and CXCL16 from brain metastasis CAFs attract cancer cells more effectively than normal fibroblasts or primary tumor CAFs, we utilized patient specific cancer cells or MCF-Her2 in a hydrogel migration assay. Each aggregate was embedded in hydrogel solution to maintain its overall 3D structure. Shown in Figure 4A is a schematic representation for cancer cell migration in vitro and an example photograph of CAF aggregates in the hydrogel with a MCF-Her2 cell line or patient specific cancer cells embedded in the center. Based on live cell imaging, immunofluorescent microscopy, and FACS analysis, we found that significantly higher numbers of MCF-Her2 cells or patient-specific cancer cells migrated to brain metastatic CAF aggregates than primary CAF or normal breast fibroblasts aggregates (Figure 4B and 4C).

To further explore the chemotactic activity of primary or brain metastatic CAF aggregates, we generated PKH labeled primary (red color) or brain metastatic (blue color) CAF aggregates mixed with green color labeled patient-derived breast cancer cells (1:1 ratio) and positioned these aggregates against a separate CAF aggregate without cancer cells within the Hydrogel (Figure 4D). This hydrogel system maintains the architecture of 3-D aggregates and also allows cancer cell migration and invasion to distant locations. We consistently observed that cancer cells mixed with primary tumor CAFs migrated towards brain metastasis CAF aggregates. Interestingly, this migration took a longer period of time than the earlier results observed in Figure 4A and B, suggesting that cancer cells were still being partially attracted by primary tumor CAFs as they migrated towards brain metastasis CAFs. These data confirm that brain metastasis CAFs promote migration of breast cancer cells more effectively than normal fibroblasts or primary tumor CAFs.

CXCR4 antagonist and CXCL16 neutralizing antibody treatments reduce cancer cell recruitment

To further investigate the importance of chemokines CXCL12 and CXCL16 secreted by CAFs on breast cancer cell recruitment, we analyzed the expression of cognate chemokine receptorsCXCR4 and CXCR6 on patient-specific cancer cells. FACS analysis showed that patient-specific breast cancer cells expressed both CXCR4 and CXCR6 (Figure 5A). Utilizing our hydrogel assay system, patient-derived breast cancer cells were treated with a receptor-blocking antagonist directed against CXCR4 alone or in combination with neutralizing antibody directed against CXCL16and tested for cancer cell migration to brain metastatic CAF aggregates. Here we utilized anti-human CXCL16 antibody since no small molecule or antagonist is not available for blocking CXCR6-CXCL16 interactions to date (*32*). Indeed, CXCR4 antagonist treatment significantly reduced the ability of cancer cells to migrate to brain metastatic CAF aggregates. The efficacy of preventing cancer cell migration cells by CXCL16 antibody treatment was less effective than CXCR4 antagonist treatment alone (Figure 5B and 5C). However, the combination of both inhibitors resulted in blocking cancer cell migration more significantly. These data confirm that production of CXCL12 and CXCL16 plays a critical role in recruiting patient-specific cancer cells to the brain metastatic microenvironment.

In summary, this is the first report demonstrating the expression of both CXCL16 and CXCL12 in human CAFs derived from breast cancer metastasis in the brain. Furthermore, neutralizing antibody directed against CXCL16, alone or in combination with CXCR4 antagonist, significantly inhibited the migration of patient-specific breast cancer cells in our 3D CAF aggregate system. The unique expression of CXCL16 by brain metastasis CAFs provides an important area of cancer research that will further our understanding of metastatic progression. Our results demonstrate the importance of understanding the specific role of CAFs on metastatic progression and possible strategies to target chemokine interactions to prevent the recruitment of circulating breast cancer cells to the brain.

Plans for the next 12 months:

- Create an *ex vivo* 3-D cell aggregate containing E007 cancer cells and MSCs derived from C57BL/6 bone marrow and implanting the 3-D aggregates under the skin of C57BL/6 mice and assess engraftment. Following engraftment, one of the aggregates will be cryo-ablated to stimulate APCs and T cell activation and cytotoxicity will be assessed.
- Utilizing the 3D CAF aggregate system, we will elucidate the methods by which stroma protects cancer cells from the efficacy of immunotherapeutic drugs.
- Monitor effect of modulation of DC clustering/maturation by testing known agents previously investigated and mentioned above, by utilizing assays in 3D aggregate cultures and 3D hydrogel matrix systems.

Supporting Data/Figures:

Table 1. Characterization of breast cancer patients

Number of Patients	Median Age of Patients	Mean Age of Patients					
5	32	37					
Sample	**Type**	**Molecular Subtype (ER, PR, Her2)**	**Tumor Grade**	**Cancer Stage**	**Age**	**BRCA**	**Surgical Reason**
BC56	Normal				48	(+)	
BC78	Normal				32	(+)	normal from contralaterial side of BC patient
BC82	Normal				32		Prophylactic mastectomy
BC97	Normal				47		
BC 131	Normal				25	(+)	
Number of Patients	**Median Age of Patients**	**Mean Age of Patients**					
8	58	55					
Sample	**Type**	**Molecular Subtype (ER, PR, Her2)**	**Tumor Grade**	**Cancer Stage**	**Age**		
BC68	Primary	(+), (+), (-)	II	IA	64		
BC80	Primary	(+), (+), (-)	III	IIA	29		
BC84	Primary	(+), (-), (-)	III		72		
BC 95	Primary	(+), (-), (+)	III	IA	50		
BC105	Primary	(+), (+), (-)	III	IIA	71		
BC108	Primary	(+), (+), (-)	II	IIA	39		
BC153	Primary	(+), (+), (-)	I	IIIA	59		
BC155	Primary	(+), (+), (-)	II	IIB	57		
Number of Patients	**Median Age of Patients**	**Mean Age of Patients**					
7	59	59					
Sample	**Type**	**Molecular Subtype (ER, PR, Her2)**	**Tumor Grade**	**Cancer Stage**	**Age**		
BC25	Brain Met	(-), (-), (+)			66		
BC55	Brain Met	(-), (-), (+)			54		
BC66	Brain Met	(+), (+), (+)			52		
BC70	Brain Met	(+), (+), (-)			63		
BC 122	Brain Met	(+), (+), (+)			59		
BC137	Brain Met	(+), (+), (-)			54		
BC 156	Brain Met	(-), (-), (+)			62		

Table 2. Cytokines and growth factors that are differentially expressed between normal stroma aggregates and brain met CAF aggregates. Genes are ranked on fold change, where a negative fold change indicates higher expression in normal stroma.

Normal vs. Met Cytokines and Growth Factors

Symbol	Entrez Gene Name	Exp p-value	Exp Fold Change
CX3CL1	C-X3-C motif chemokine ligand 1	0.000	256.042
AGT	angiotensinogen	0.000	247.041
PGF	placental growth factor	0.000	12.237
PDGFA	platelet derived growth factor subunit A	0.000	8.859
EBI3	Epstein-Barr virus induced 3	0.125	6.428
FGF10	fibroblast growth factor 10	0.252	5.572
TGFB2	transforming growth factor beta 2	0.002	5.390
CXCL16	C-X-C motif chemokine ligand 16	0.001	5.341
NRG2	neuregulin 2	0.125	5.279
PTN	pleiotrophin	0.000	5.036
SCG2	secretogranin II	0.048	4.850
NDP	Norrie disease (pseudoglioma)	0.031	4.664
EREG	epiregulin	0.219	4.589
FGF1	fibroblast growth factor 1	0.125	3.496
ANGPT1	angiopoietin 1	0.059	2.795
TGFB3	transforming growth factor beta 3	0.132	2.274
DKK3	dickkopf WNT signaling pathway inhibitor 3	0.129	1.855
CXCL12	C-X-C motif chemokine ligand 12	0.069	1.814
CCL5	C-C motif chemokine ligand 5	1.000	1.366
CCL7	C-C motif chemokine ligand 7	0.780	-1.486
LIF	leukemia inhibitory factor	0.263	-1.499
FGF2	fibroblast growth factor 2	0.283	-1.536
HBEGF	heparin binding EGF like growth factor	0.507	-1.589
CLEC11A	C-type lectin domain family 11 member A	0.025	-1.654
CTF1	cardiotrophin 1	0.441	-1.720
WNT5A	Wnt family member 5A	0.251	-1.770
LEP	leptin	0.597	-1.802
TNF	tumor necrosis factor	1.000	-1.809
CXCL8	C-X-C motif chemokine ligand 8	0.232	-2.158
GAS6	growth arrest specific 6	0.017	-2.221
NGF	nerve growth factor	0.060	-2.231
GDNF	glial cell derived neurotrophic factor	0.143	-2.253
VEGFC	vascular endothelial growth factor C	0.013	-2.273
INHBA	inhibin beta A	0.083	-2.294
IL33	interleukin 33	0.071	-2.367
CXCL3	C-X-C motif chemokine ligand 3	0.236	-2.383
BMP6	bone morphogenetic protein 6	0.453	-2.396
IL11	interleukin 11	0.217	-2.427
CXCL2	C-X-C motif chemokine ligand 2	0.259	-2.578
SPP1	secreted phosphoprotein 1	0.005	-2.735
DKK1	dickkopf WNT signaling pathway inhibitor 1	0.041	-2.809
IL6	interleukin 6	0.075	-2.901
FGF7	fibroblast growth factor 7	0.055	-3.568

Normal vs. Primary Cytokines and Growth Factors

Symbol	Entrez Gene Name	Exp p-value	Exp Fold Change
OGN	osteoglycin	0.000	20.174
FGF10	fibroblast growth factor 10	0.002	18.125
TGFB2	transforming growth factor beta 2	0.000	8.068
CXCL10	C-X-C motif chemokine ligand 10	0.013	7.120
NDP	Norrie disease (pseudoglioma)	0.080	3.952
HGF	hepatocyte growth factor	0.003	2.838
CCL7	C-C motif chemokine ligand 7	0.154	2.457
BMP2	bone morphogenetic protein 2	0.143	2.200
MDK	midkine (neurite growth-promoting factor 2)	0.013	2.151
KITLG	KIT ligand	0.059	1.634
NAMPT	nicotinamide phosphoribosyltransferase	0.257	1.576
PROK1	prokineticin 1	1.000	1.519
TYMP	thymidine phosphorylase	0.245	1.488
NOV	nephroblastoma overexpressed	0.191	-1.680
WNT5A	Wnt family member 5A	0.293	-1.713
VEGFC	vascular endothelial growth factor C	0.042	-1.963
SPP1	secreted phosphoprotein 1	0.015	-2.348
NGF	nerve growth factor	0.038	-2.544
INHBA	inhibin beta A	0.023	-3.036
LIF	leukemia inhibitory factor	0.003	-3.077
CXCL8	C-X-C motif chemokine ligand 8	0.056	-3.549
CXCL3	C-X-C motif chemokine ligand 3	0.102	-3.912
DKK1	dickkopf WNT signaling pathway inhibitor 1	0.008	-4.189
IL11	interleukin 11	0.051	-4.379
CTGF	connective tissue growth factor	0.002	-4.490
CCL3	C-C motif chemokine ligand 3	0.250	-5.041
IL1B	interleukin 1 beta	0.127	-5.061
IL24	interleukin 24	0.138	-6.299
IL6	interleukin 6	0.001	-8.292
CXCL2	C-X-C motif chemokine ligand 2	0.010	-10.812
CSF3	colony stimulating factor 3	0.011	-15.910

Primary vs. Met Cytokines and Growth Factors

Symbol	Entrez Gene Name	Exp p-value	Exp Fold Change
CX3CL1	C-X3-C motif chemokine ligand 1	0.000	323.562
AGT	angiotensinogen	0.000	120.006
PGF	placental growth factor	0.000	12.799
PDGFA	platelet derived growth factor subunit A	0.000	10.296
FGF1	fibroblast growth factor 1	0.031	7.398
SCG2	secretogranin II	0.016	7.100
EREG	epiregulin	0.063	6.756
CXCL16	C-X-C motif chemokine ligand 16	0.001	6.436
CSF3	colony stimulating factor 3	0.098	6.097
CTGF	connective tissue growth factor	0.000	5.356
EBI3	Epstein-Barr virus induced 3	0.125	5.299
NRG2	neuregulin 2	0.125	5.278
IL1B	interleukin 1 beta	0.127	4.753
CXCL2	C-X-C motif chemokine ligand 2	0.117	4.194
PTN	pleiotrophin	0.000	3.671
ANGPT1	angiopoietin 1	0.027	3.549
IL6	interleukin 6	0.139	2.858
TNFSF13B	tumor necrosis factor superfamily member 13b	0.228	2.333
LIF	leukemia inhibitory factor	0.063	2.052
INHBB	inhibin beta B	1.000	1.873
CXCL12	C-X-C motif chemokine ligand 12	0.139	1.609
IL15	interleukin 15	1.000	1.563
EDN1	endothelin 1	1.000	1.474
TGFB2	transforming growth factor beta 2	0.411	-1.497
TIMP1	TIMP metallopeptidase inhibitor 1	0.026	-1.509
CTF1	cardiotrophin 1	0.441	-1.580
CLEC11A	C-type lectin domain family 11 member A	0.025	-1.656
IL32	interleukin 32	0.249	-1.662
GAS6	growth arrest specific 6	0.118	-1.692
IL33	interleukin 33	0.224	-1.821
KITLG	KIT ligand	0.009	-1.992
HGF	hepatocyte growth factor	0.024	-2.179
TYMP	thymidine phosphorylase	0.020	-2.217
NAMPT	nicotinamide phosphoribosyltransferase	0.038	-2.337
CXCL6	C-X-C motif chemokine ligand 6	0.180	-2.552
MDK	midkine (neurite growth-promoting factor 2)	0.001	-2.837
CXCL10	C-X-C motif chemokine ligand 10	0.098	-3.106
FGF10	fibroblast growth factor 10	0.097	-3.253
BMP2	bone morphogenetic protein 2	0.024	-3.523
IL1RN	interleukin 1 receptor antagonist	0.081	-3.586
CCL7	C-C motif chemokine ligand 7	0.053	-3.651
FGF7	fibroblast growth factor 7	0.025	-4.264
OGN	osteoglycin	0.002	-9.248

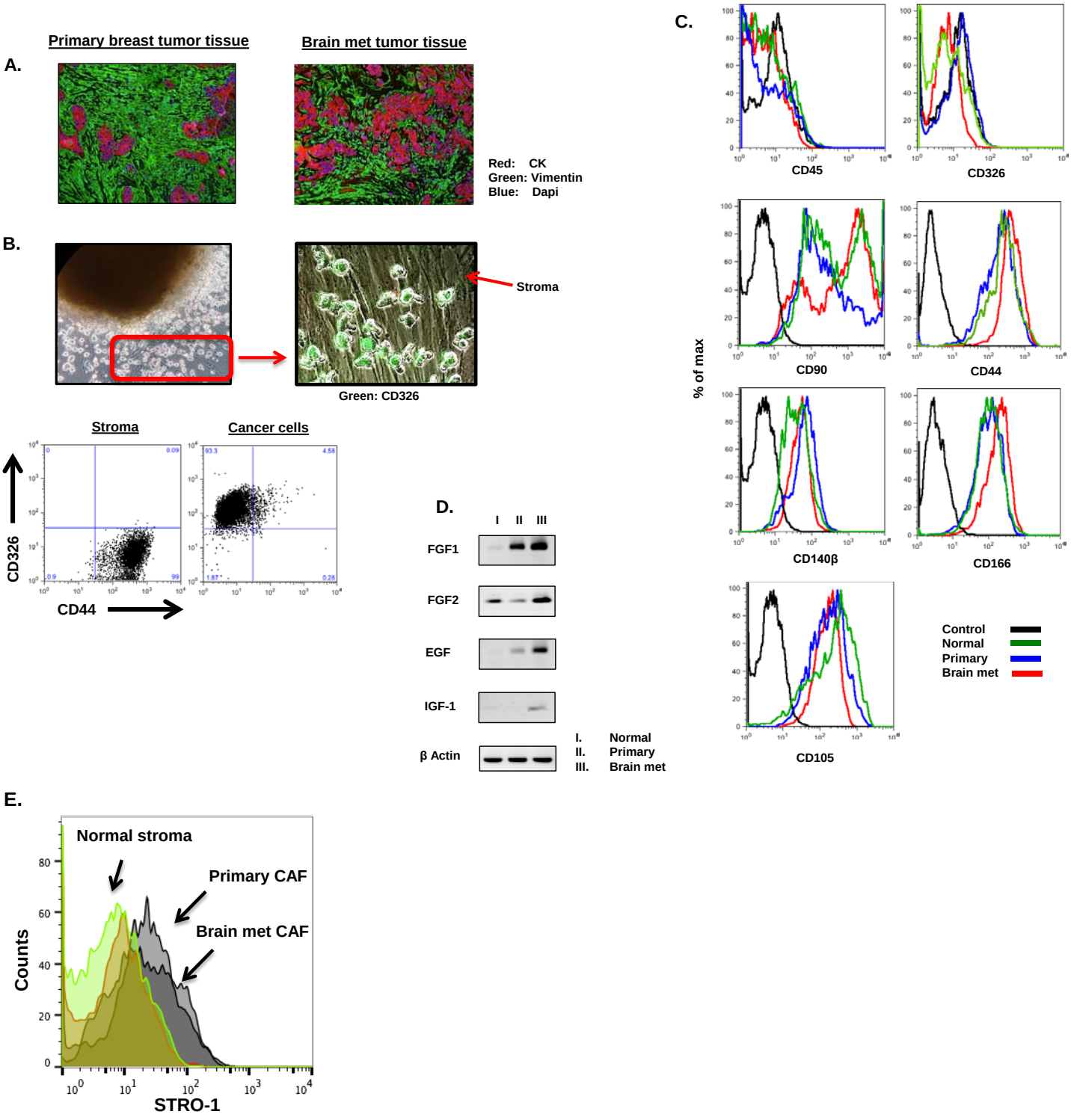

Figure 1. Characterization of fibroblasts isolated from primary and brain met breast tumor in culture. (A) Immunohistochemistry was performed to determine the prevalence of cancer-associated fibroblasts (vimentin+) surrounding breast cancer cells (CK+). (B) Morphology of cancer associated fibroblasts (CAF) and breast cancer cells growing in tissue culture, 2 weeks after plating human breast tumor fragments (green color represents CD326+ cancer cells and a red arrow indicates CD326- CD45- fibroblasts). (C) At 2 to 4 weeks, normal human breast fibroblast, primary CAF, and brain met CAS surface marker expression was analyzed by FACS. (D) Gel Electrophoresis RT PCR data demonstrates relative growth factor expression of FGF-1, FGF-2, EGF, and IGF-1 in normal, primary and metastatic aggregate stroma. (E) Representative images of CAF tissue culture show that both primary and brain met stroma populations contain STRO-1+ (MSC marker) expressing cells.

A.

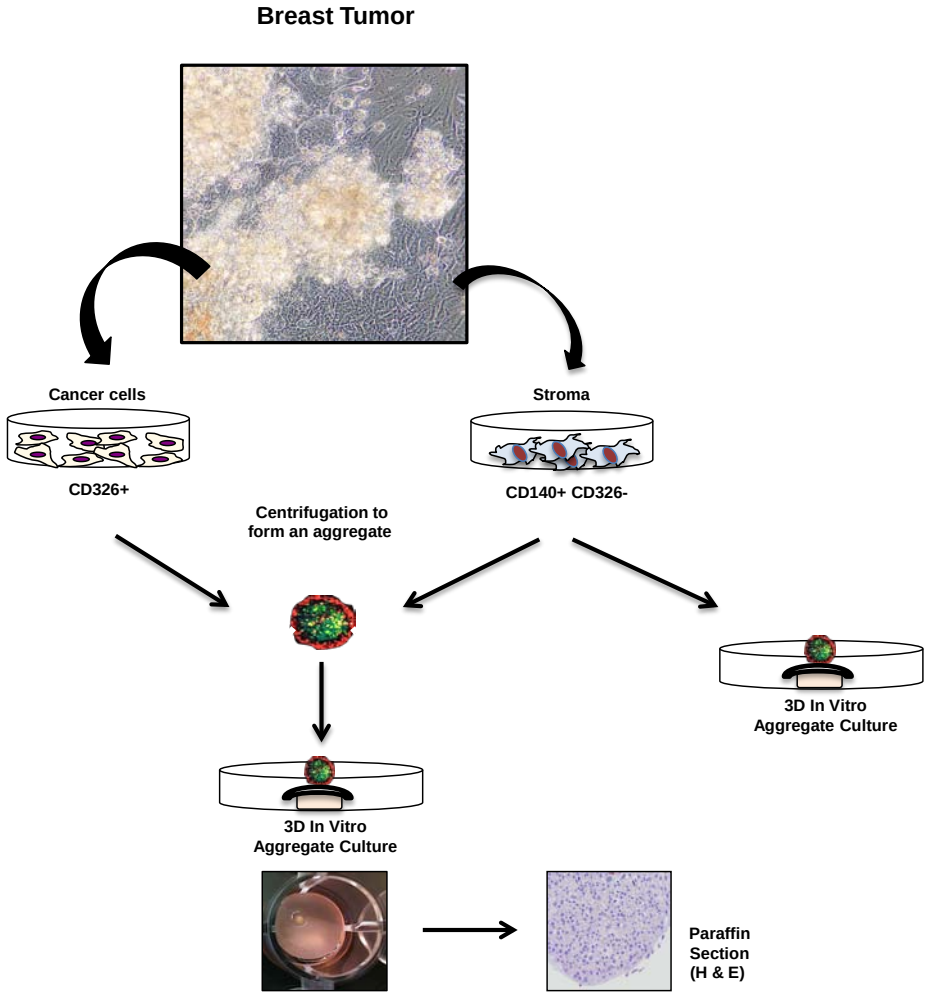
Breast Tumor
Cancer cells
CD326+
Stroma
CD140+ CD326-
Centrifugation to form an aggregate
3D In Vitro Aggregate Culture
3D In Vitro Aggregate Culture
Paraffin Section (H & E)

B.

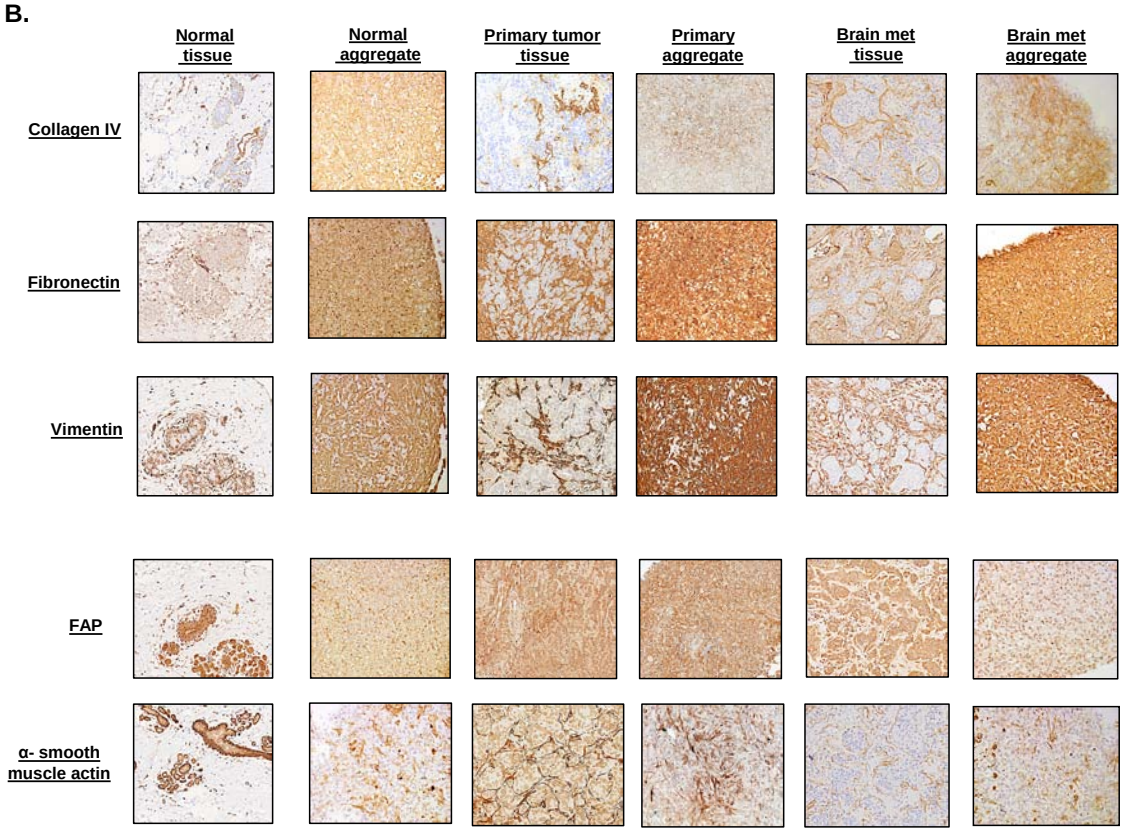
Normal tissue
Normal aggregate
Primary tumor tissue
Primary aggregate
Brain met tissue
Brain met aggregate
Collagen IV
Fibronectin
Vimentin
FAP
α- smooth muscle actin

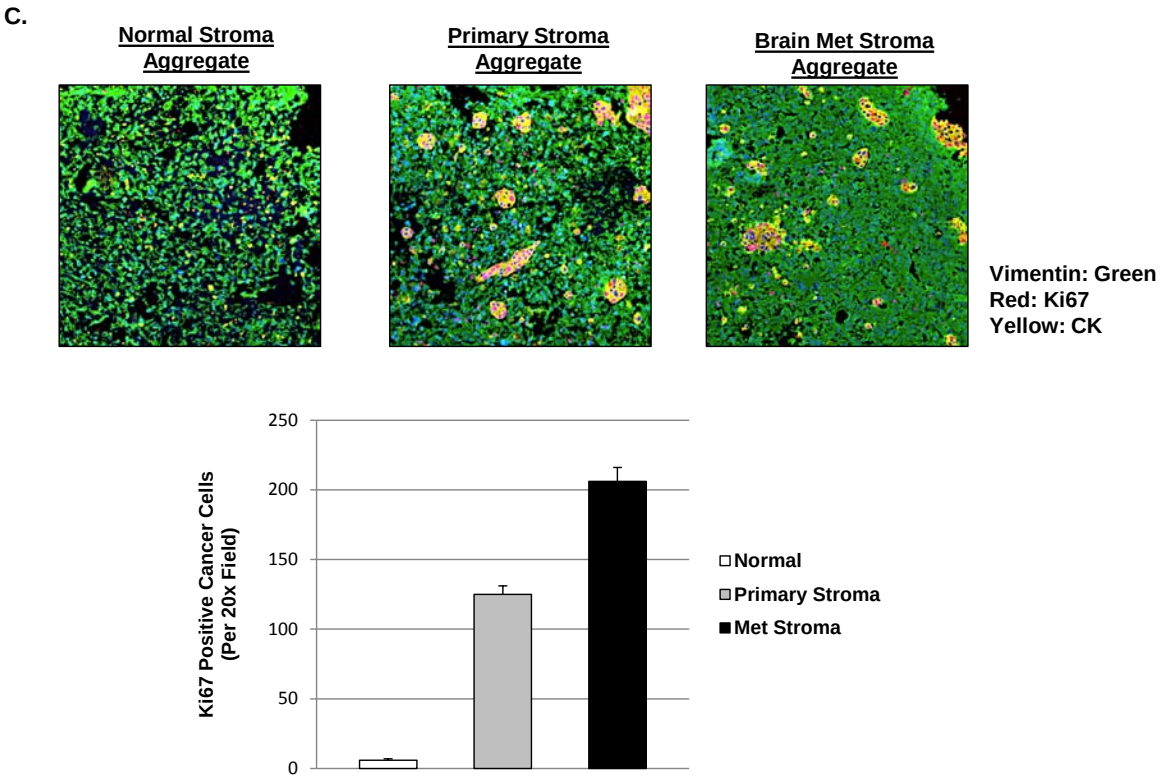

Figure 2. Generation of 3-D human breast cancer microenvironment in vitro.
(A) Schematic representation for generation of 3-D human breast stroma aggregates for in vitro model. Human breast cancer associated breast stromal cells were generated from patient specific primary or brain met tumor tissues ex vivo. Aggregates were then cultured on nucleopore membranes floating in D10 medium supplemented with human epidermal growth factor (hEGF) for 2 weeks for in vitro analyses. (B) Immunohistochemical staining comparison between human breast cancer tissues and cancer associated stromal aggregates. Paraffin-embedded stromal aggregates were sectioned and stained for vimentin and activated fibroblast markers including alpha smooth muscle and fibroblast activating protein (FAP). Expression of extra-cellular matrix (ECM) components was analyzed in both tissue section and aggregates. Antibody staining directed against fibronectin and collagen IV showed the presence of ECM in all aggregates. (C) Immuno-fluorescent antibody staining against Ki67 (Red), cytokeratin (Yellow) and vimentin (Green) in patient-derived aggregates composed of cancer cells mixed with either normal, primary or metastatic stroma. Bar graph illustrates relative expression of Ki67 in cancer cells from normal, primary or metastatic stroma patient samples.

A.

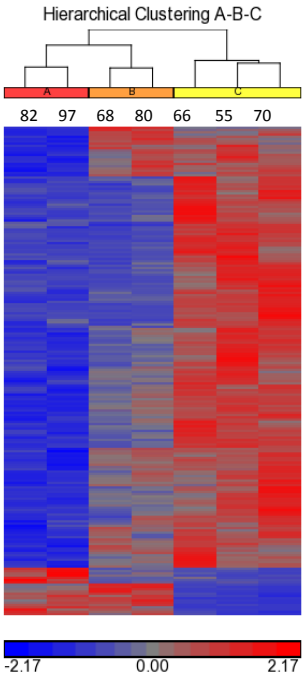

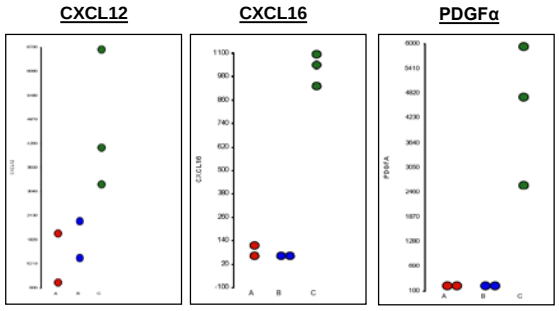

B.

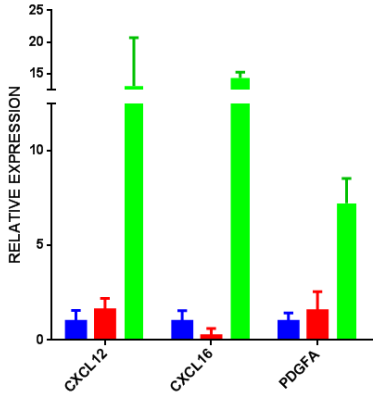

C.

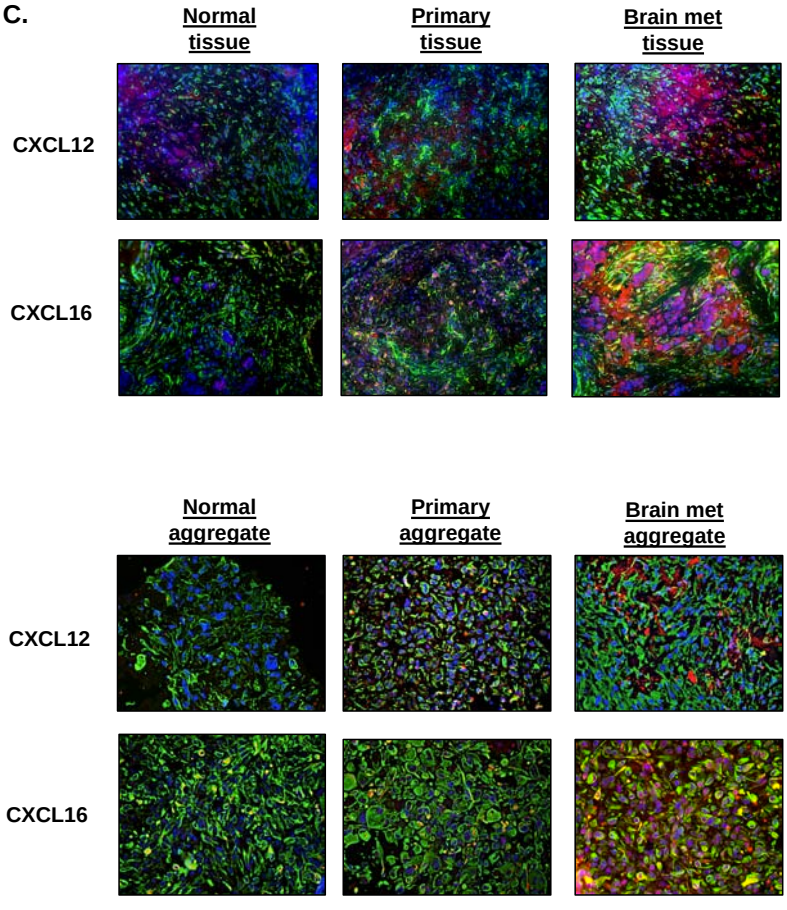

Red: CXCL12 or CXCL16
Green: Vimentin

D.

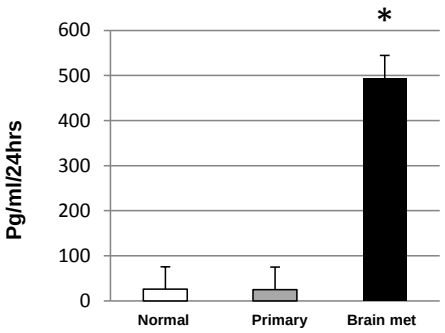

Figure 3. Gene and protein expression analyses of 3-D human breast cancer CAF aggregates.
(A) Heat map of hierarchical cluster analysis of RNA seq data derived from the normal, primary breast tumor CAF, and brain met CAF aggregates. BC82 and BC97 were used for the normal aggregate group, BC68 and BC80 were used for the primary aggregate group, and BC66, BC70 and BC55 were used for the brain met aggregate group (see Table 1). Individual gene dot plots showing changes in mean expression levels of transcripts PDGFα, CXCL12, and CXCL16. (B) Quantitative RT-PCR validation of relative changes in expression levels of the CXCL12, CXCL16, and PDGFα. (C) Immuno-fluorescent staining directed against CXCL12 and CXCL16 expression from patient tissue and patient-derived CAF aggregate. Representative immunofluorescent images show Vimentin (green) and CXCL12/CXCL16 (red) expression in both patient-derived tissue and patient-derived stromal aggregates. Scale bar for zoomed images represent 50μm. (D) Measurement of soluble CXCL16 in media of patient derived normal, primary and metastatic stroma by ELISA. Metastatic & Primary Stroma: ($^{\#}P< 0.03$): Metastatic & Primary Stroma: ($^{\#}P< 0.03$).

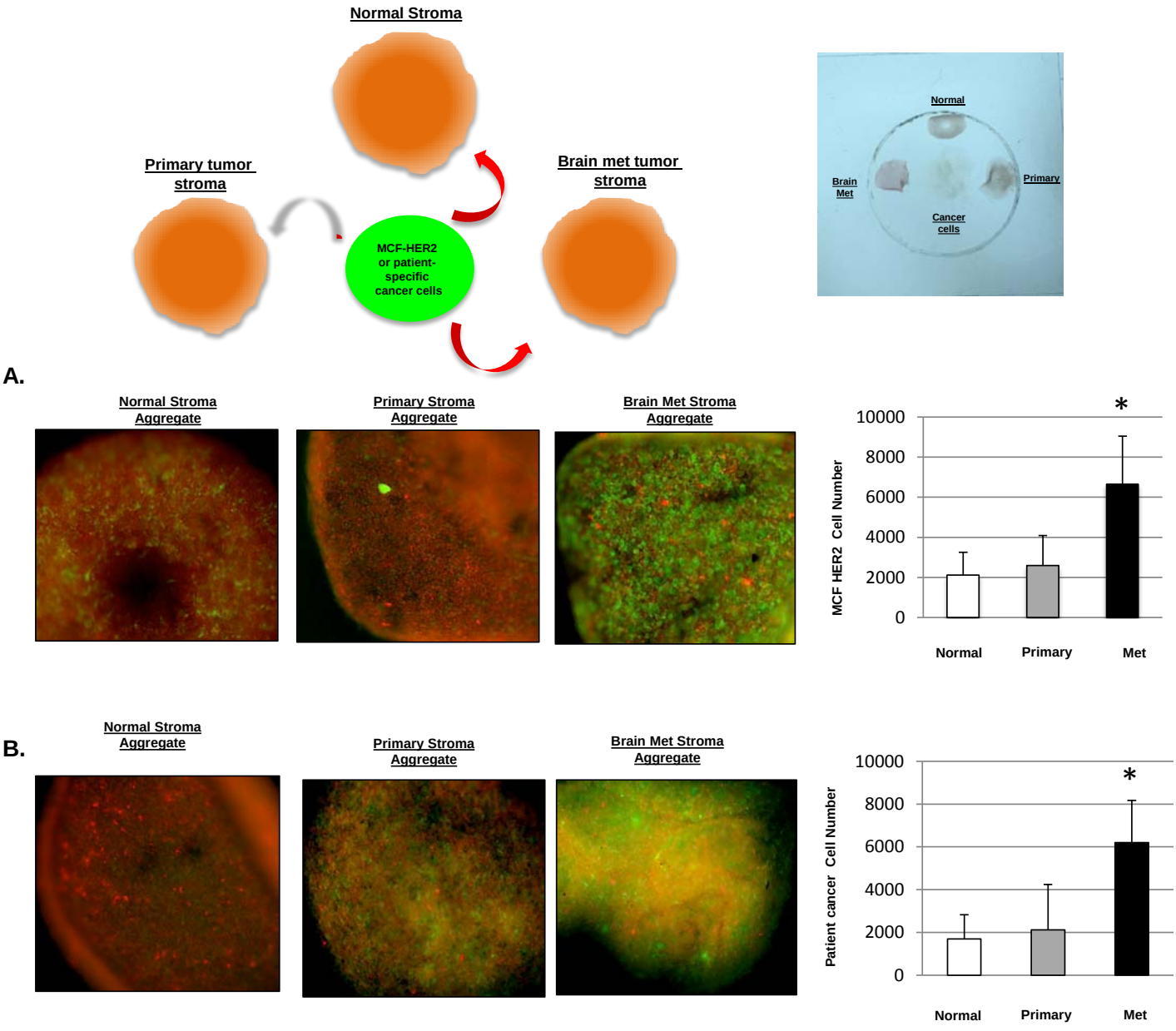

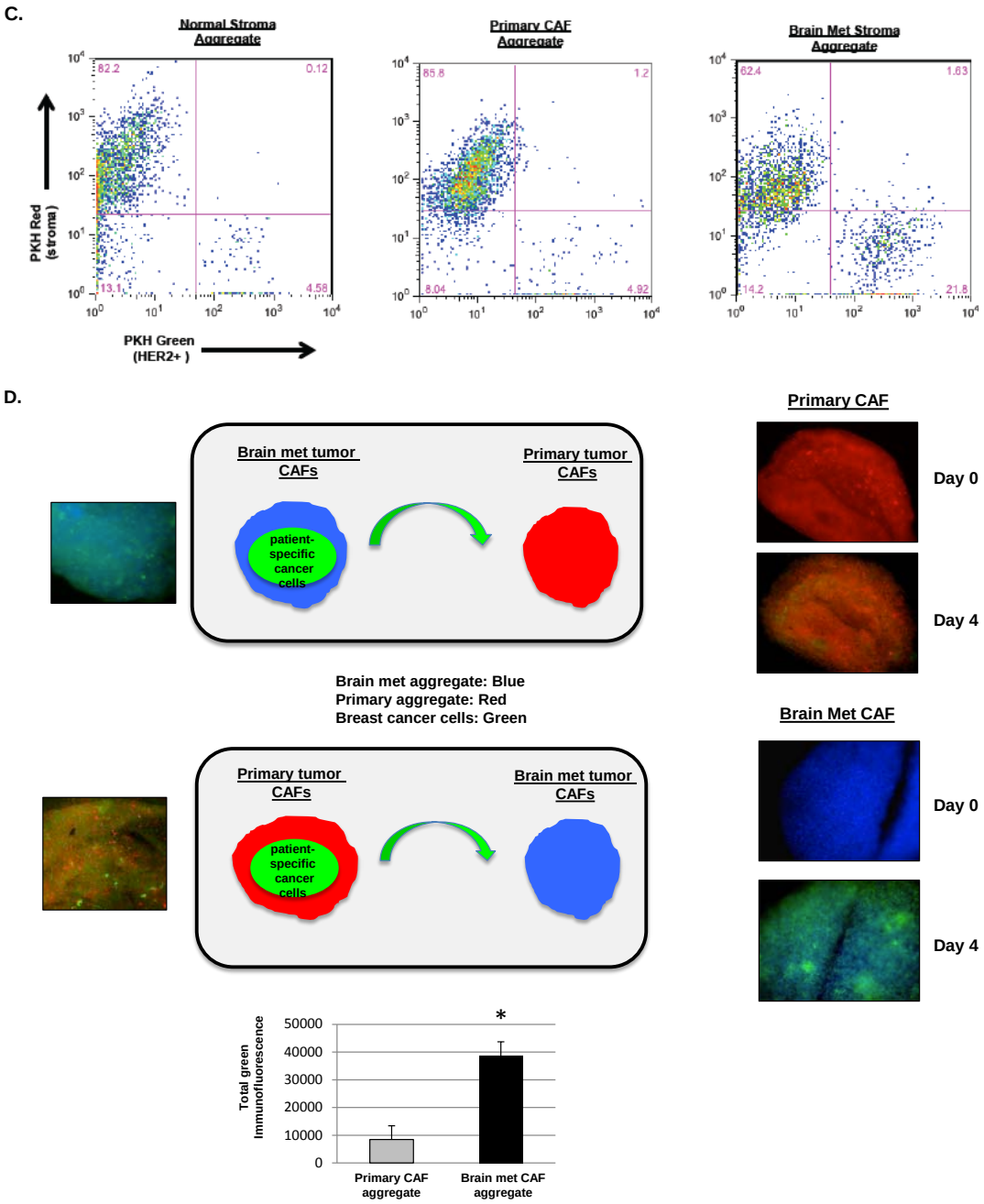

Figure 4. Effects of CAF in migration of cancer cells in vitro.
(A) Immuno-fluorescent images comparing migration of cancer cell line MCF-Her2 (Red) to either normal, primary or metastatic patient-derived CAF aggregate. Bar graph quantifies relative migration of Her-2+ (CD340+) cancer cells to normal (BC69, BC82, BC97, and BC102), primary (BC80, BC95, BC105, and BC108), or metastatic (BC25, BC55, BC66, and BC70) CAF aggregate independently (see Table 1). (B) Immunofluorescent images comparing migration of patient-derived cancer cells to either normal, primary or metastatic patient-derived CAF aggregate. Bar graph demonstrates relative migratory count of cancer cells to normal (BC69, BC82, BC97, and BC102), primary (BC80, BC95, BC105, and BC108), or metastatic (BC25, BC55, BC66, and BC70) CAF aggregate independently. (C) FACS analysis showing the relative migration of PKH green-labeled cancer cells to normal, primary or metastatic patient aggregates that were labeled with PKH red.24 hours post-incubation, higher percentage of patient-specific cancer cells migrated to brain metastatic CAF aggregates than primary CAF or normal breast fibroblasts aggregates. (D) Immuno-fluorescent images compare migration of patient-specific cancer cells (green) towards either Primary CAF (Red) or brain metastasis CAF (*34*) on Day 0 and Day 4. Bar graph quantifies relative total cell fluorescence of patient-specific cancer cells that have migrated to primary or brain metastatic CAF aggregate. ($^{\#}P< 0.01$)

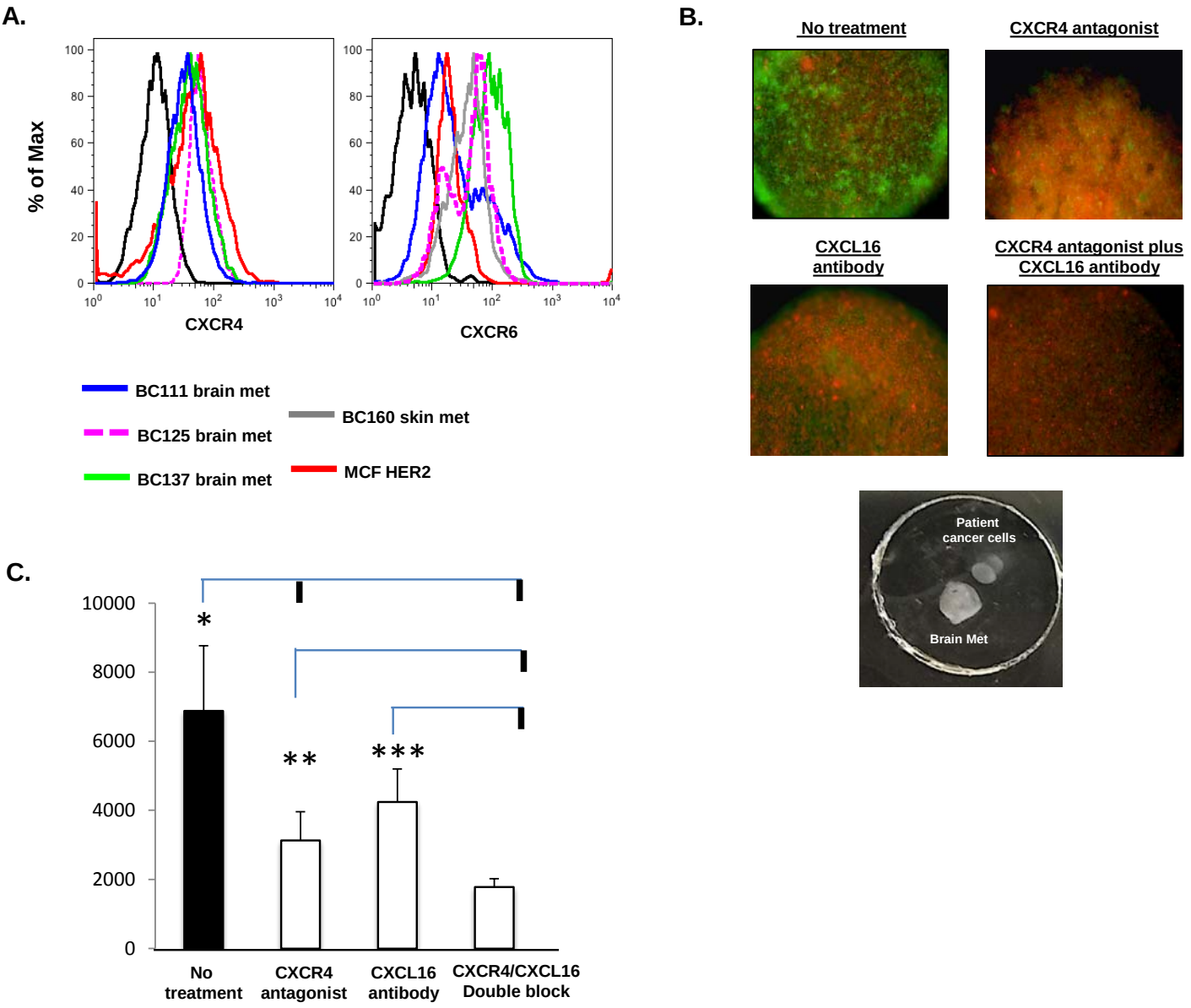

Figure 5. Combination of CXCR4 antagonist and CXCL16 neutralizing antibody treatment reduces cancer cell recruitment

(A) FACS analysis of relative CXCR4 or CXCR6 expression on cancer cell line MCF-Her2 and patient-specific cancer cells derived from brain metastasis or skin metastasis tissue. (B) Immuno-fluorescent images demonstrate relative migration of patient-specific cancer cells (green) to brain metastasis stroma (Red) with or without CXCR4 antagonist and CXCL16 neutralization in Hydrogel-Migration assay. (C) Bar graph quantifies the relative migration of patient specific cancer cells that have been untreated or treated with CXCR4 antagonist, CXCL16 neutralization antibody, or a combination of both agents. An asterisk indicates significant differences between groups of animals (*P ≤ 0.02; **P ≤ 0.045; ***P ≤ 0.02). Each value represents the mean of 3-5 independent experiments. For the migration assay, BC25, BC55, BC66, BC70 brain metastatic CAF aggregates were independently utilized (see Table 1). Consistent results were obtained in repeated experiments throughout. The vertical bold lines branching off from the top of the horizontal lines represent statistically significant *P* values when the untreated, CXCR4 antagonist, and CXCL16 neutralizing antibody groups were individually compared with all other groups.

Task 2. Investigate mechanisms by which chronic IL6 affects immune function: months 1-36.

2a. Gene expression analyses and flow cytometry to measure expression of positive and negative signaling regulators (month 1-60).

2b. T cell polarization and functional assays (month 1-60).

Multiple immune defects have been documented in cancer patients, which limit the ability of the host immune response to control cancer progression and metastases to prevent relapse. In addition, tumor-promoting immune functions have been shown to be up-regulated in cancer patients. The universal dysfunction of the immune system could be explained by a breakdown in communication via cytokines. IL-6 is a cytokine that signals through a receptor complex of GP130 and IL-6Ra to activate the STAT3 and STAT1 transcription factors (*35*). IL-6 has pleiotropic roles in disease and immune responses with a well-known role in promoting tumorigenesis. In cancer settings, IL-6 is produced by tumor cells, tumor stroma and tumor-associated myeloid cells and activates phosphorylation of STAT3 (pSTAT3) in tumor cells to promote survival and proliferation. STAT3 itself is considered an oncogene and also promotes the renewal of cancer stem cells (*36*).

Breast cancer patients are known to have elevated serum levels of IL-6, and higher serum IL-6 levels are associated with poorer survival in metastatic breast cancer patients (*37, 38*). Because of the strongly supported role of IL-6 in promoting tumorigenesis, multiple efforts are underway to inhibit IL-6 as a therapeutic intervention. For immune cells, IL-6 has vital roles in T cell activation, for instance by inhibiting T_{REG} while promoting T_H17 differentiation (*39*). Mice lacking IL-6 are unable to elicit effective immune responses against viruses and bacteria (*34, 40*). T cells from breast cancer patients are known to have impaired effector functions and are skewed towards T_{REG} populations. However the role of IL-6 in breast cancer patient T cell function has not been previously addressed. IL-27 also signals through GP130 paired with a unique receptor WSX-1 to activate STAT1 and STAT3 (*41*). IL-27 is known to enhance T_H1 and inhibit T_H2 polarization by synergizing with IL12 to promote IFNɣ production and inhibiting T_H2 cytokine production (*42-44*). IL-27 was also shown to induce generation of effector CTLs from naive $CD8^+$ T cells in a STAT1-dependant manner (*45, 46*). Interestingly, IL-27 has anti-tumor activities *in vivo* in mice (*47*).

While both IL-6 and IL-27 activate STAT1 and STAT3, IL-6 tends to favor STAT3 activation, and IL-27 favors STAT1. STAT1 and STAT3 cross-regulate one another by competing for binding sites on cytokine receptors, upregulating expression of negative regulators, and can form heterodimers to alter promoter binding specificities (*48*). STAT1 and STAT3 mediate opposing effects on both tumor cell survival and immune cell activity. In tumor cells, STAT3 promotes survival and proliferation. In contrast, STAT1 promotes cell cycle arrest and apoptosis (*48*). In immune cells, cytokines, including IL-10 and VEGF, activate STAT3-mediated immune suppression, while STAT1 activation promotes antigen presentation, inflammatory responses, and T_H1 immunity (*48*). Immune cells lacking STAT3 exhibit enhanced tumor immune-surveillance (*49, 50*). These studies indicate the crucial balance of cytokine signaling in directing anti-tumor immune responses.

<u>Gene expression analysis to measure expression of positive and negative signaling regulators</u>

To investigate whether the impaired IL-6 signaling response was caused by reduced levels of the IL-6 receptor complex, we compared the cell surface levels of IL-6Rα and gp130 in naïve $CD4^+$ T cells between BC patients and healthy donors by flow cytometry. Indeed, we found that IL-6Rα ($p=0.05$) and gp130 ($p=0.03$) levels were both lower in BC patients than in healthy donors (Fig. 1A). In addition, IL-6 induced pSTATs significantly correlate with the level of IL-6Rα plus gp130 (pSTAT1: $p=0.0005$; pSTAT3: $p=0.0009$) (Fig. 1B). Within the tumor microenvironment, IL-6 is well-established as a pro-tumor cytokine and high expression levels of IL-6 are found within human BC tumors (*37, 51, 52*). Previous studies demonstrated that chronic exposure to IL-6 causes reduced levels of gp130 on T cells (*53-55*). To address whether these changes were regulated at the transcriptional level, we measured the mRNA levels of IL-6Rα and gp130 in $CD4^+$ naïve T cells by qPCR. Indeed, mRNA levels of gp130 (*Il6st*) ($p=0.04$) were significantly lower in T cells from BC patients ($n=4$) than in healthy donors ($n=4$), but not IL-6Rα (*Il6r*) (Fig. 1C). IL-6Rα on the cell surface is known to be subjected to proteolytic cleavage by a metallopeptidase ADAM 17 (*56*). Intriguingly, we found that mRNA

levels of ADAM17 were significantly higher (p=0.03) in T cells from BC patients than healthy donors (Fig. 1C). These data indicate that impaired IL-6 signaling responses in T cells from BC patients are caused by reductions in both chains of the IL-6 receptor complex via two distinct mechanisms: gp130 via reduced transcription, and IL-6Rα via enhanced cleavage by ADAM17.

Functional consequences of impaired IL-6 signaling in Th17 cell polarization

IL-6 functions include promoting T cell survival, mediating helper T cell differentiation decisions by promoting Th2 over Th1 induction and Th17 over Treg induction, and regulating chemokine receptor expression, thereby influencing T cell recruitment to tissues (*57, 58*). Therefore, loss of IL-6 responses may result in dysfunctional T cell survival as well as altered helper T cell differentiation and recruitment during inflammatory conditions. In the presence of IL-6 and TGFβ and IL-1β, naïve T cells can differentiate into Th17 cells, which are characterized by expression of the master transcription factor RORγt (*59*). Th17 cells are found to negatively correlate with the presence of Treg cells and positively correlate with effector immune cells, including cytotoxic $CD8^+$ T cells and NK cells (*60, 61*). The anti-tumor role of Th17 cells is at least partially due to their capacity to recruit effector cytotoxic T cells. Since IL-6 is critical for Th17 differentiation (*39*), we examined whether dysfunctional IL-6 signaling responses in naïve T cells from BC patients was associated with impaired Th17 differentiation. Naïve $CD4^+$ T cells were isolated from fresh PBMCs and cultured in Th17 differentiation medium for 7 days. BC patient samples (n=7) exhibited fewer differentiated Th17 cells ($ROR\gamma t^+IL\text{-}17A^+$) (p=0.02) (Fig. 2A) with lower IL-17 secretion levels (p=0.04) (Fig. 2B) than age-matched healthy donors (n=9). Among the BC patients, IL-6 induced pSTATs significantly correlated with levels of IL-17 production (pSTAT1: p=0.001; pSTAT3: p=0.03) (Fig. 2C).

IL-27 signaling response dysregulation and the association with clinical outcome in BC

IL-27 is mainly produced by activated APCs including DCs and macrophages. IL-27 is essential for the interaction between the innate and adaptive arms of antitumor immunity. IL-27 leads to the differentiation of Th1 cells through phosphorylation of STAT1 and T-bet activation. In addition, IL-27 synergizes with IL-12 to enhance IFNγ production. Moreover, it has been shown that IL-27 inhibits Th2 polarization of naive CD4+ T cells and suppresses the production of Th2 cytokines from in vitro polarized Th2 cells. In Th2 cells, IL-27-mediated activation of STAT1 and T-bet suppresses the transcription factor GATA-3. By altering the balance between Th1/Th2 cytokines, IL-27 is critically important in antitumor immune responses (7, 62-67).
To determine if IL-27 responses are altered similarly to IL-6, phosphoflow cytometry was used to measure the IL-27 induced activation of STAT1 and BC patient PBMCs compared with healthy controls. We found that IL-27 induced phosphorylation of STAT1 in naïve CD4+ T cells from BC patients was significantly lower than that in healthy donors (Fig. 3A). To evaluate whether IL-27 signaling significantly correlates with clinical outcome, Kaplan-Meier survival analysis was performed to determine the relationship between IL-27 signaling responses and relapse-free survival (RFS). To divide BC patients into two populations in an unbiased way, median ΔMFI of IL-27 induced pSTAT1 was used as the cut-off. However, the correlation between IL-27 signaling and RFS was not significant (Fig. 3B).

IL-10 signaling response dysregulation and the association with clinical outcome in BC

IL-10, a cytokine produced by almost all leukocytes, is primarily a potent anti-inflammatory cytokine that inhibits gene expression and T cell/macrophage cytokine synthesis and inhibits their antigen-presenting capacity. IL-10 also inhibits IFN-γ synthesis by activated Th-cells and PBMC and induces mast cell proliferation. The IL-10/IL-10R interaction activates tyrosine kinases, and these kinases are responsible for the phosphorylation of tyrosine residues within the intracellular domain of IL-10R1 which serve as docking sites for STATs. IL-10 rapidly activates STAT3 and it remains phosphorylated over a sustained period (*68*).

We examined IL-10 signaling response in CD8 T cells and found that IL-10 induced phosphorylation of STAT3 in CD8 T cells from BC patients was significantly higher than that in healthy donors (Fig 4A). To evaluate whether IL-10 signaling significantly correlates with clinical outcome, Kaplan-Meier survival analysis was performed to determine the relationship between IL-10 signaling responses and relapse-free survival (RFS).

To divide BC patients into two populations in an unbiased way, median ΔMFI of IL-10 induced pSTAT3 was used as the cut-off. However, the correlation between IL-10 signaling and RFS was not significant (Fig. 4B).

IFNγ signaling response dysregulation and the association with clinical outcome in BC

Potential mechanisms of immune dysfunction in cancer include defects in antigen recognition (first signal), costimulation (second signal), and cytokines, (e.g., IFNs; third signal). Efficient IFN signaling is critical to provide the third signal to enable full activation, clonal expansion, and memory development rather than tolerance, and for efficient natural killer (NK)-cell-mediated cytotoxicity. Efficient IFNγ signaling is critical to immune function and we hypothesized that altered IFNγ signaling may be a key mechanism of immune dysfunction common to cancer (*69*).

To investigate IFNγ immune biology in BC patients, we analyzed the responsiveness of peripheral blood immune cells to IFNγ in BC patients and age-matched healthy donors. We examined IFNγ signaling response in T cells ($CD3^+$), B cells ($CD20^+$), NK cells ($CD16^+$) and myeloid cells ($CD33^+$) and found that IFNγ induced phosphorylation of STAT1 in $CD33^+$ myeloid cells from BC patients was significantly lower than that in healthy donors (Fig. 5A). To evaluate whether IFNγ signaling significantly correlates with clinical outcome, Kaplan-Meier survival analysis was performed to determine the relationship between IFNγ signaling responses and relapse-free survival (RFS). To divide BC patients into two populations in an unbiased way, median ΔMFI of IFNγ induced pSTAT1 was used as the cut-off. We found that BC patients with pSTAT1 ΔMFI below the median had significantly worse RFS than those above the median ΔMFI (Fig. 5B), indicating that lower IFNγ signaling responses in peripheral $CD33^+$ myeloid cells predict worse RFS. In addition, we also found a significantly correlation between signaling response to IFNγ and IL-6 (Fig 6. A-B), suggesting that BC patients with lower signaling response to IFNγ in $CD33^+$ myeloid cells tend to have lower signaling response to IL-6 in CD4 naïve T cells.

Plans for the next 12 months:

- Determine the functional consequences caused by these dysregulated cytokine signaling responses in peripheral blood immune cells.

- Investigate whether signaling responses of immune-suppressive cytokine TGFβ are dysregulated in breast cancer patients.

Supporting Data/Figures:

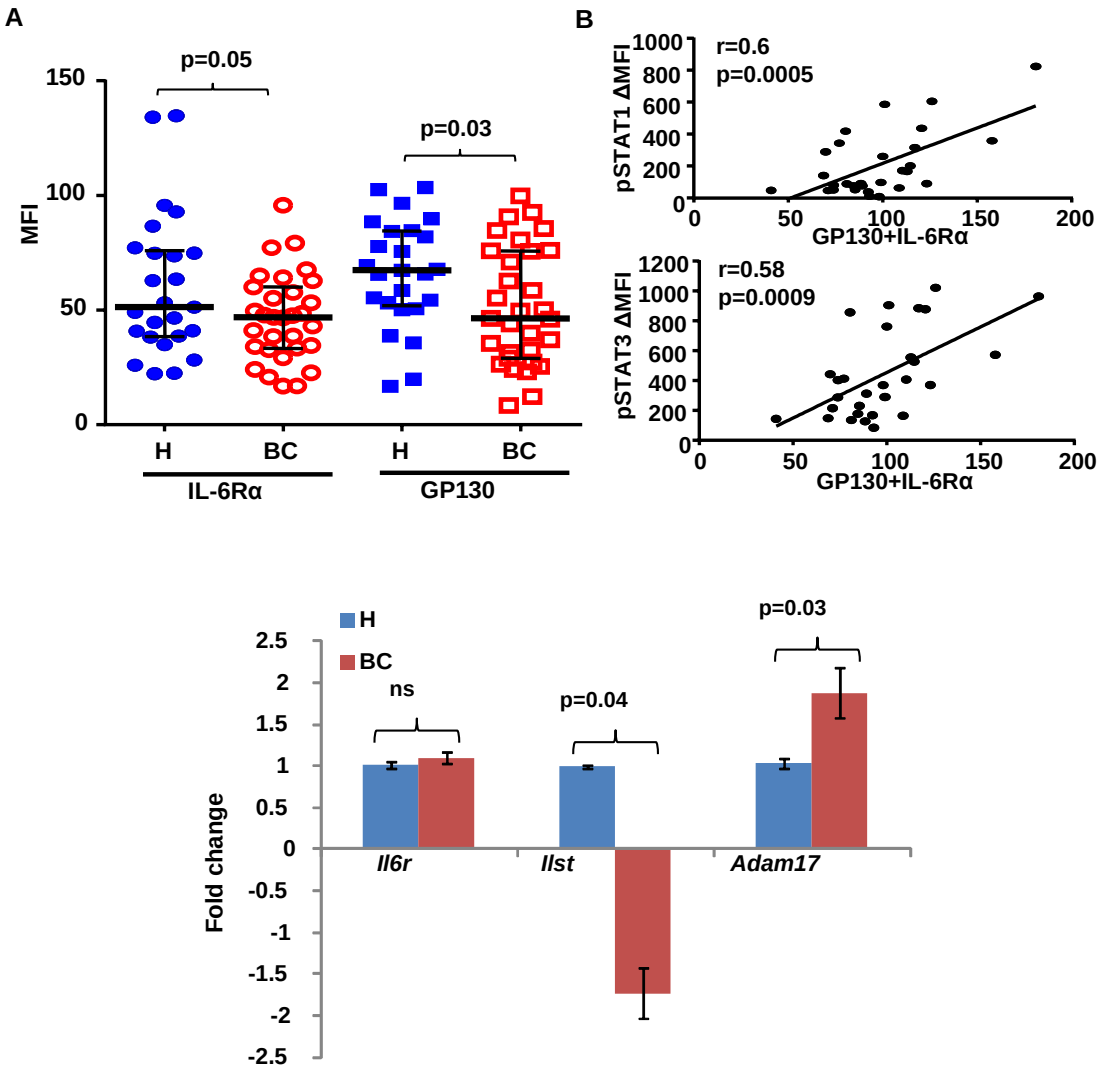

Figure 1. Impaired IL-6 signaling responses in naïve CD4$^+$ T cells is associated with lower IL-6 receptor levels.

(A) Surface expression levels of IL-6Rα (p=0.05) and gp130 (p=0.03) on naïve CD4$^+$ T cells from healthy donors (n=25) and BC patients (n=31) were determined by flow cytometry with anti-IL-6Rα and anti-gp130 antibodies. (B) The associations between IL-6 induced pSTATs and the expression levels of gp130 plus IL-6Rα were determined by Pearson's correlation coefficient test (pSTAT1: r=0.6, p=0.0005; pSTAT3: r=0.58, p=0.0009). (C) Total RNA was extracted from isolated CD4$^+$ naïve T cells and analyzed for the relative fold change by Q-PCR. mRNA levels of IL-6Rα (*Il6r*) (p=ns), gp130 (*Il6st*) (p=0.04) and ADAM17 (*Adam17*) (p=0.03) were compared between healthy donors (n=4) and BC patients (n=4).

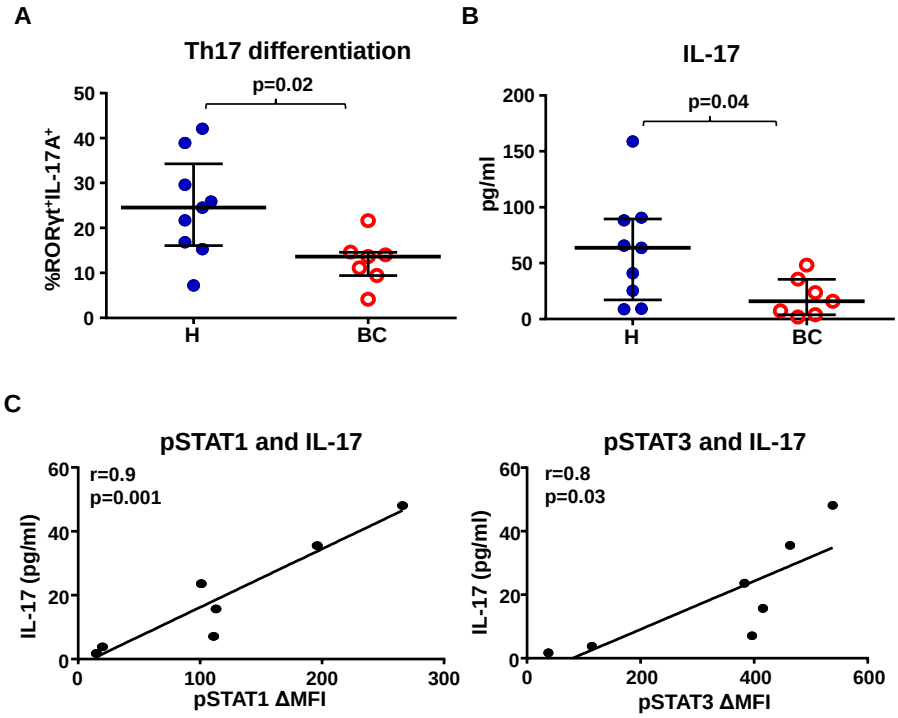

Figure 2. Impaired IL-6 signaling responses in naïve CD4$^+$ T cells is associated with defective Th17 differentiation.

(A) Naïve CD4$^+$ T cells were isolated from fresh PBMCs and were cultured in Th17 differentiation medium for 7 days. RORγt$^+$IL-17A$^+$ cells identified Th17 cells by flow cytometry. The percentages of differentiated Th17 cells were compared between BC patients (n=7) and age-matched healthy donors (n=8). (p=0.02). (B) Supernatants were collected after 7 days of Th17 differentiation and the levels of IL-17 were determined by ELISA (pg/ml/1×10^6 cells). The levels of IL-17 were compared between BC patients (n=7) and age-matched healthy donors (n=9). (p=0.04). (C) Among the BC patients (n=7), the associations between IL-6 induced pSTATs and level of IL-17 were determined by Pearson's correlation coefficient test. (pSTAT1: r=0.9, p=0.001; pSTAT3: r=0.8, p=0.03).

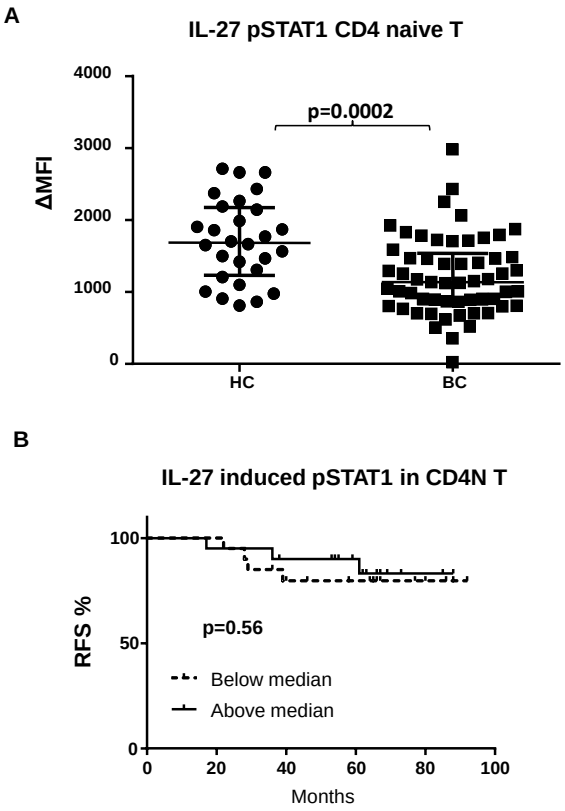

Figure 3. IL-27 signaling response is impaired in peripheral naïve CD4$^+$ T cells from BC patients.
(A) IL-27 induced phosphorylation of STAT1 (p=0.0002) in peripheral naïve CD4$^+$ T cells were compared between BC patients and age-matched healthy donors. (B) Kaplan-Meier survival analysis was performed to compare relapse-free survival (RFS) between BC patients with lower and higher IL-27 signaling response. The median IL-27 induced phosphorylation of STAT1 (ΔMFI) was used as the cut-off to divide BC patients into lower and higher IL-27 signaling response groups.

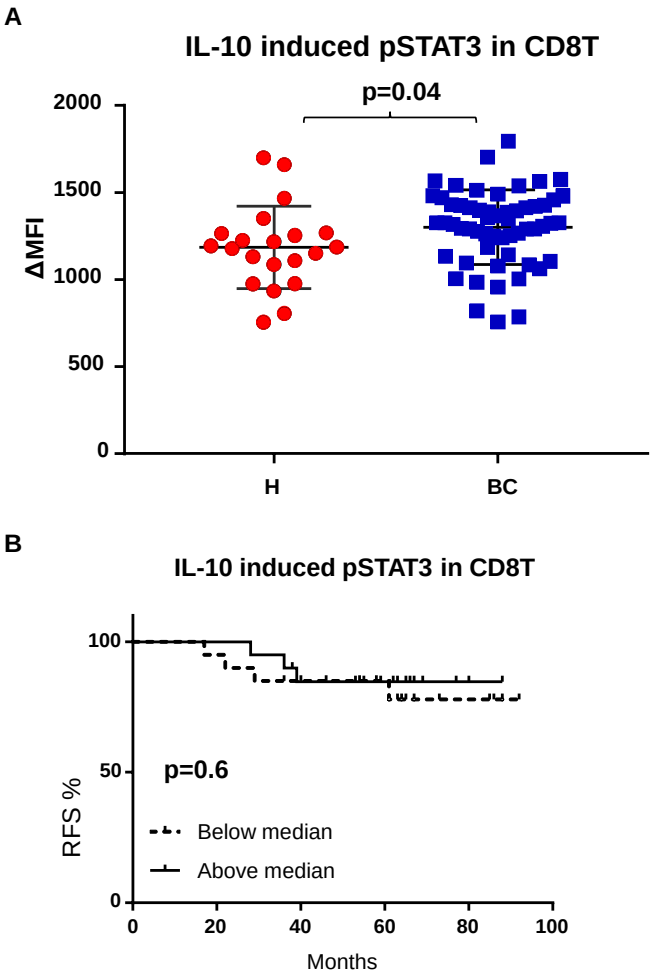

Figure 4. IL-10 signaling response is impaired in peripheral naïve CD8+ T cells from BC patients.
(A) IL-10 induced phosphorylation of STAT3 (p=0.04) in peripheral CD8+ T cells were compared between BC patients and age-matched healthy donors. (B) Kaplan-Meier survival analysis was performed to compare relapse-free survival (RFS) between BC patients with lower and higher IL-10 signaling response. The median IL-10 induced phosphorylation of STAT3 (ΔMFI) was used as the cut-off to divide BC patients into lower and higher IL-10 signaling response groups.

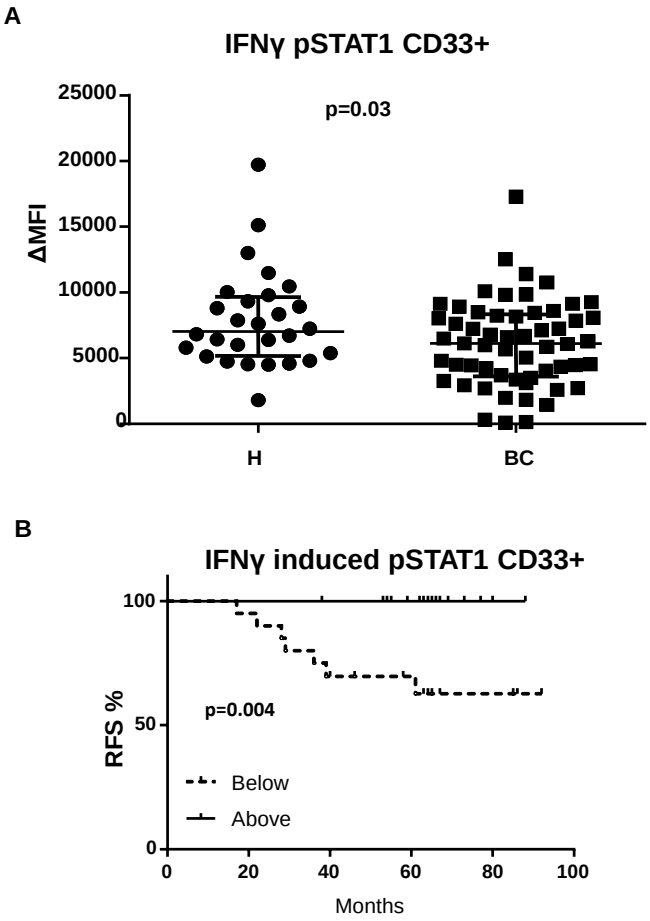

Figure 5. IFNγ signaling response is impaired in peripheral CD33+ myeloid cells from BC patients.
(A) IFNγ induced phosphorylation of STAT1 (p=0.03) in peripheral CD33+ myeloid cells were compared between BC patients and age-matched healthy donors. (B) Kaplan-Meier survival analysis was performed to compare relapse-free survival (RFS) between BC patients with lower and higher IFNγ signaling response. The median IFNγ induced phosphorylation of STAT1 (ΔMFI) was used as the cut-off to divide BC patients into lower and higher IFNγ signaling response groups.

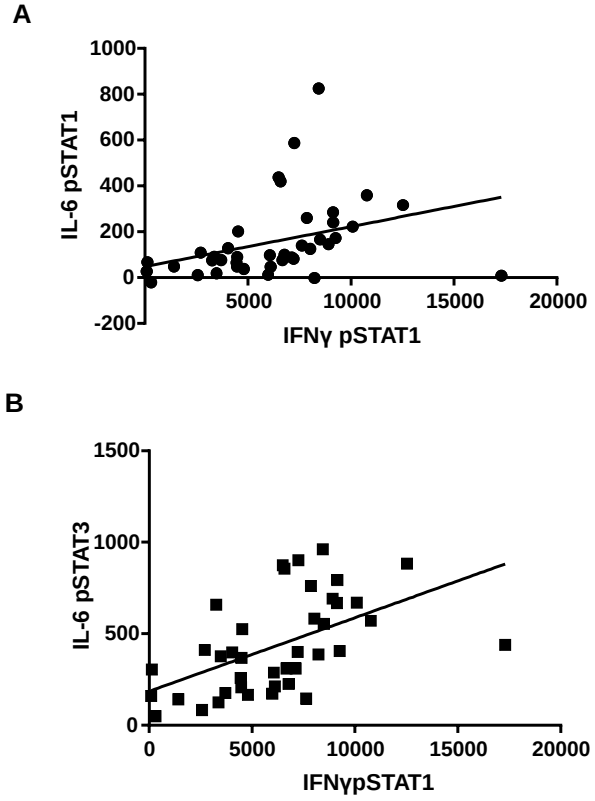

Figure 6. The association between IL-6 induced pSTAT1 (A) and pSTAT3 (B) in naïve $CD4^+$ T cells and IFNγ induced pSTAT1 in CD33+ myeloid cells from BC patients were determined by Pearson's correlation coefficient test.

Task 3. Select Optimal Integrated Immunotherapy Combinations in Animal Models for Clinical Development: months 12-60.

3a. Optimize post-surgical murine model of breast cancer metastasis (month 12-36).

3b. DC vaccination optimization by restoration of DC clustering and maturation (months 24-48).

3c. Optimization of the amplification and effector phases by correcting chronic IL6-mediated defective T cell responses . (month 24-48).

3d. Combining optimal DC vaccination strategies with cytokine signaling modulation therapeutics for optimal immunotherapeutic regimens (month 36-60).

3e. Testing other strategies and combinations. (month 48-60).

While some combinations of FDA approved cytokine therapeutics for cancer (IL-2 and IFN-α2b) have shown modest incremental efficacy, they have been limited by substantial toxicities (*70*). Previous cytokines tested clinically as cancer therapeutics were selected based on putative effects to enhance immune function rather than specifically to correct immune signaling defects in cancer. In addition, DC vaccination effectiveness may be hampered by an immunosuppressive environment, which prevents maturation and clustering in lymph nodes. Each of the key phases of the immune response—induction, amplification, and effector immune cell generation—is defective in breast cancer patients, so it follows that integrated immunotherapy combinations that address all of the phases of the normal immune response will be much more effective than individual treatments that address only one mechanism.

Developing integrated immunotherapeutic regimens to target the immune signaling defects that occur in each phase of the immune response, in combination with optimal DC-vaccination strategies using immunologically validated antigens, will generate highly functional and prolonged anti-tumor immune responses in breast cancer patients that will prevent recurrence and metastasis.

We will focus on developing a thorough approach to best take our findings about the 3D tumor microenvironment and its unique setting with our knowledge of cytokine signaling functions in immune and cancer cells and then attempt to assess *in vivo* effectiveness of combining the regimens for induction of optimal anti-tumor immunity. Then we will determine the optimal time to administer these regimens during disease progression, with and without chemotherapy. As surgery removes the primary tumor burden, we will focus our studies on the post-surgical setting where we envision immunotherapy is most effective to eradicate micrometastases to prevent relapse.

Ivermectin synergizes with autophagy inducing drugs by compromising protective P2X4/P2X7/Pannexin-1 signaling in cancer cells

The phenomenon of immunogenic cell death (ICD) has recently attracted significant attention due to the realization that cytotoxic therapies inducing concurrent specific and durable anti-tumor immune responses possess superior therapeutic potential (*71, 72*). Moreover, synergistic drug combinations utilizing cardiac glycosides were shown to convert a non-immunogenic cell death into classical ICD, demonstrating the feasibility of using potent drug synergy as a platform for integrated cancer immunotherapy (*73, 74*). ICD has been mechanistically linked to surface exposure of calreticulin (CRT) and the release of nuclear HMGB1. The third key component of ICD is the autophagy-associated release of extracellular ATP originating from autophagosome/lysosomes and opening of the P2X4/P2X7-gated plasma membrane Pannexin-1 channels (*75-77*). Interestingly, P2X7 expression has been positively correlated with tumor growth and responses to doxorubicin (*1, 78, 79*). We have recently shown that the FDA-approved anti-parasitic drug Ivermectin can modulate P2X4/P2X7/Pannexin-1 channel activity, over-activating a normally protective cellular mechanism and converting it into a P2X7/CAMKII/MPTP-dependent cytotoxic pathway that drives an inflammatory and mixed apoptotic/necrotic cancer cell death manifesting all of the characteristics of ICD (*80*). Here we

demonstrate that Ivermectin-based synergistic drug combinations have significant therapeutic potential. Ivermectin was found to be synergistic with other known modulators of the P2X4/P2X7/Pannexin-1/NLRP3/Caspase-1 pathway, as well as with a number of clinically relevant therapeutics that are known to induce autophagy through mechanistically diverse mechanisms. Autophagy and apoptosis are important homeostatic mechanisms that consume large amounts of ATP to provide chemo-resistance and immunologically silent cell death, respectively (*81*). Importantly, we found that the synergy between Ivermectin and doxorubicin was dependent on autophagy and could be attributed to the ability of lower and more physiologically relevant doses of Ivermectin to compromise cellular ATP metabolism and to abolish the protective functions of purinergic signaling mediated by P2X7 receptors, Pannexin-1 channels, and CAMKII activity.

Ivermectin-based synergistic combinations are effective against triple-negative breast cancer

We previously showed that Ivermectin is active as a single agent against triple-negative breast cancer (TNBC), and now extend this work to combinations of Ivermectin with other anti-cancer agents. Combination of Ivermectin with doxorubicin induced cell death in both human and mouse TNBC cell lines at a lower concentration than either of them alone (Figure 1A). Synergy between these drugs was also validated with colony experiments under physiologically relevant extended low-dose conditions (Figure 1B). Synergy was seen over a wide range of concentrations, except for short 24h exposure to lower doses of doxorubicin, suggesting that drug synergy *in vivo* might require maintenance of effective doses of both Ivermectin and doxorubicin.

We next sought to determine if the combination of Ivermectin and doxorubicin has anti-tumor effect *in vivo*. The route of Ivermectin administration can influence the outcome of treatments so we first tested whether systemic oral treatment was better than direct intratumoral administration. Interestingly, direct intra-tumoral injection of Ivermectin, aimed at achieving higher local cytotoxic drug concentrations, had the same effect as untreated (naïve) or vehicle alone (Figure 1C), while orally administered Ivermectin had statistically significant anti-tumor effects as a single agent. These data demonstrate that Ivermectin has anti-tumor activity in vivo but intratumoral injection may be to subject to fast diffusion or recruitment of tumor promoting factors/cell populations. In subject experiments, mice treated with orally administered Ivermectin had similar anti-tumor effects as doxorubicin alone, and importantly, the combination of Ivermectin and doxorubicin demonstrated superior therapeutic potential compared to Ivermectin or doxorubicin alone (Figure 1D). Tumor protection could not be further improved using higher doses of Ivermectin, which became toxic when applied for one week or longer (data not shown). These *in vivo* data suggest that Ivermectin-based synergistic drug combinations might be feasible in breast and other types of solid tumors, but require careful dosing of the drugs.

Synergy between doxorubicin and Ivermectin is dependent on autophagy

Previously, we demonstrated the potential of Ivermectin to kill breast cancer cells through over-activation of the otherwise protective P2X4/P2X7/Pannexin-1 pathway, which also plays a central role in autophagy-induced ATP release and ICD. To investigate the potential involvement of autophagy in the mechanism of Ivermectin and doxorubcin synergy, we tested their ability to kill wild type vs. autophagy deficient shRNA(Atg5)/(Beclin-1) MDA-MB-231 breast cancer cells (Figure 2A). Autophagy deficiency lowered the EC50 values for doxorubicin, consistent with the expected protective role of autophagy in conferring resistance to chemotherapy (Figure 2B). Interestingly, autophagy deficiency compromised the synergy between doxorubicin and Ivermectin at the most cytotoxic doses of doxorubicin (Figure 2C), suggesting that Ivermectin might impact the balance between protective and cytotoxic roles of autophagy.

Ivermectin is synergistic with molecular targeted therapeutics

We also investigated the potential of Ivermectin to synergize with molecular targeted therapeutic agents. Agents tested can be separated into several groups including: **1.** Drugs that directly target the AKT/MTOR signaling pathway, such as rapamycin and wortmannin (Figure 3A and 3B, respectively); **2.** Drugs that impact the AKT/MTOR pathway by modulating vital growth factor signaling such as EGFR inhibitors (Figures 3C); **3.** Drugs that reportedly target MTOR through activation of AMPK, such as resveratrol (Figure 3D) (*82*). Ivermectin was found to be synergistic with higher doses of all of these agents. This broad synergistic potential could be simply attributed to simultaneous suppression of Akt signaling because Ivermectin was found to

induce phosphorylation of AKT (Figure 3E). Furthermore, treatment with Ivermectin in the presence of Wortmannin, which inhibits the phosphorylation of AKT, exacerbated killing indicating the protective role of AKT signaling.

Ivermectin is synergistic with other modulators of the P2X4/P2X7/Pannexin-1/NLRP3/Caspase-1 pathway

We next investigated whether compromised autophagy-associated protective mechanisms can be linked to the Ivermectin-sensitive P2X4/P2X7/Pannexin-1 pathway, which is a major player in both autophagy and ICD. The low affinity P2X7 agonist ATPγS did not synergize with Ivermectin and was actually antagonistic, consistent with the dual transiently protective role of ATP demonstrated by us previously (Figure 4A) (*80*). Ivermectin was, however, synergistic with the potent P2X7 agonist Bz-ATP and a novel liver X receptor (LXR) agonist that was recently shown to modulate Pannexin-1 channel activity promoting a necrotic form of cancer cell death through downstream NLRP3 inflammasome and caspase-1 activation (Figure 4B) (*83*). Interestingly, clearance of NLRP3 inflammasomes and down-regulation of caspase-1 activation appeared to be dependent on another regulator of autophagy - the proteasome. We found that proteasome inhibitors indeed promote cancer cell death in the context of caspase-1 (but not caspase-3) activation (Figure 4C, data not shown). Combining Ivermectin with bortesomib or carfilisomib augmented caspase-1 activation and was highly synergistic and superior to other autophagy inducing drugs (Figure 4D, 4E). These synergies provide further support to the hypothesis that Ivermectin targets the P2X4/P2X7/Pannexin-1/NLRP3/Caspase-1 pathway in cancer.

Ivermectin compromises the protective functions of ATP release and purinergic signaling mediated by P2X7 receptors, Pannexin-1 channels and CAMKII

The P2X4/P2X7/Pannexin-1 pathway is involved in both autophagy and ICD. This prompted us to investigate whether Ivermectin sensitizes tumor cells to doxorubicin by compromising protective mechanisms dependent on autophagy-associated extracellular ATP release involving the P2X4/P2X7/Pannexin-1 signaling. It has been shown that Ivermectin can enhance the accumulation of doxorubicin and other chemotherapeutic agents through modulation of MDR-1 (*84, 85*) so we first tested if Ivermectin also enhanced doxorubicin uptake in breast cancer cells. When 4T1.2 and MB231 cells were treated with Ivermectin, accumulation of doxorubicin was increased in both cell lines (Figure 5A), despite the fact that Ivermectin up-regulated MDR-1 expression (data not shown). Doxorubicin resistance has also been linked to up-regulation of P2X7-receptors (*79*) and CaMKII activity (*86*), suggesting another possible mechanism by which Ivermectin might modulate resistance to doxorubicin. We found that P2X7-deficiency was indeed associated with increased accumulation of doxorubicin (Figure 5B). Further, the effect of Ivermectin on doxorubicin accumulation can be mimicked by blockade of P2X7 and CaMKII (which can regulate P2X4/P2X7-gated Pannexin-1 channels) with low doses of KN-62 and KN-93, respectively (Figure 5C, 5D). Blockade of P2X7 receptors and Pannexin-1 channels with the P2X7 receptor antagonist A438079 and Probenecid, an inhibitor of Pannexin-1 was unable to directly enhance doxorubicn accumulation but inhibited the effect of Ivermectin, further emphasizing that the P2X4/P2X7/Pannexin-1 complex plays a complicated role in the regulation of drug uptake and sensitivity. Importantly, we found that inhibition of P2X7 and CaMKII eliminated the synergy between doxorubicin and Ivermectin in both murine and human TNBC cell lines, and was mostly due to increased sensitivity to doxorubicin (Figure 5E, left). Similar roles for P2X7 and CaMKII can be observed in the context of the proteasome inhibitor Carfilizomib (Figure 5E, right). An important difference is that the elimination of protective P2X7/ CaMKII signaling does not result in a complete loss of synergy with Ivermectin, consistent with our hypothesis that Ivermectin and proteasome inhibitors might primarily synergize downstream at the NLRP3 inflammasome/Caspase-1 level. Our finding that under extended low-dose exposure Ivermectin, which is a positive allosteric modulator of P2X4 receptors, can compromise rather than potentiate P2X4/P2X7/Pannexin-1-dependent protective functions is both surprising and paradoxical. We hypothesize that such a dramatic shift in biological activity can be attributed to Ivermectin-induced changes in ATP metabolism as ATP is the other major regulator of the activity of the P2X4/P2X7/Pannexin-1 complex.

Ivermectin compromises cellular ATP metabolism

Several lines of evidence pointed to a critical role for ATP in Ivermectin induced cytotoxicity and synergy with other autophagy inducing drugs. Autophagy consumes significant amounts of cellular ATP and

released extracellular ATP is rapidly degraded to adenosine. Changes in the AMP/ATP ratio and purinergic receptors-induced Ca2+ flux are sensed by AMPK that is able to directly inhibit MTOR. Involvement of AMPK is supported by the fact that Ivermectin-induced autophagy occurs in the context of elevated rather than suppressed pAKT (pAKT) (Figure 3E), which points to the involvement of another potent negative regulator of MTOR signaling. Therefore, we wanted to determine if Ivermectin affects cytosolic ATP homeostasis. Using 4T1.2 breast cancer cells engineered to express cytosolic Luciferase, we found that extended exposure to Ivermectin resulted in a dose-dependent depletion of cytosolic ATP reserves that preceded cell death (Figure 6A). The immediate effect of Ivermectin on 4T1.2 cells within the first 4h of exposure was a transient increase in cytosolic ATP, which corresponded to the transient release of extracellular ATP and appeared to be essential for cell survival (Figure 6B) (*80*). To investigate whether depletion of ATP reserves contributes to Ivermectin cytotoxicity, we utilized inhibitors targeting major factors that consume cellular ATP during Ivermectin-induced autophagy, cytotoxic Ca2+ flux, and apoptosis: Bafilomycin A (vacuolar type H+- ATPase), Digoxin (Na+/K+ ATPase) (*80*), and Olaparib (PARP) (Figure 6C), respectively. All of these were shown to provide a transient partial protection, emphasizing the role of dynamics of ATP in all features of cell death induced by acute doses of Ivermectin.

Ivermectin induced Caspase-1 can potentially target key glycolytic enzymes and we have previously shown that Ivermectin caused transient mitochondrial hyper-polarization followed by mitochondrial permeability transition pore (MPTP) opening. Metabolic flux (Seahorse) analysis was used to clarify whether the gradual depletion of cellular ATP reserves was due not only to enhanced consumption but also to decrease in ATP generation from glycolysis and mitochondrial respiration. Ivermectin inhibited mitochondrial respiration without the compensation from glycolysis (Figure 6D, 6E). Surprisingly, blockade of the first step of glycolysis by 2-Deoxy-D-glucose (2-DG) or redirecting pyruvate to mitochondrial respiration with dichloroacetic acid (DCA) provided a modest protective effect on cells subjected to acute treatment of Ivermectin, suggesting that glycolysis might contribute to Ivermectin-induced acute cytotoxicity through accumulation of lactate, the final product of glycolysis (Figure 6F). Excessive acidification in cancer cells is normally counteracted by the activities of the Na+/H+ exchanger, the Na+/ Ca2+ exchanger, and the Na+/K+ ATPase, which can exacerbate the rise in cytosolic Ca2+ and drive over-activation of CaMKII and MPTP (*87*). Indeed, we found that lactic acid, but not lactate, -mediated cytosolic acidification can exacerbate Ivermectin cytotoxicity (Figure 6G). Overall, our data suggest that Ivermectin compromises ATP homeostasis through gradual autophagy-associated dissipation of the available ATP pool combined with interference with mitochondrial respiration that cannot be effectively compensated by glycolysis due to excessive cytosolic Ca2+ and pH imbalance. The potentiating effect of Ivermectin on P2X4/P2X7/Pannexin-1 signaling is therefore only transient and might gradually decline as the cellular ATP reserves are depleted.

Here we present novel mechanistic studies on Ivermectin, a FDA-approved anti-parasitic agent that has been reported by us and others to modulate the activity of the P2X4/P2X7/Pannexin-1/NLRP3/Caspase-1/IL-1β axis in cancer cells. We show that Ivermectin-mediated modulation of purinergic signaling can impact the balance of autophagy-dependent pro-survival and cytotoxic signals, sensitizing cancer cells to a broad spectrum of autophagy-inducing therapeutics. Our data confirm that the P2X4/P2X7/Pannexin-1 complex plays a critical role in the synergy between Ivermectin and autophagy inducing drugs like doxorubicin, suggesting that in the presence of Ivermectin, the protective mechanisms dependent on P2X7 receptors and CaMKII, including the MDR-1-mediated export of cytotoxic drugs, are dysfunctional and correlate with enhanced uptake and retention by the tumor cells and improved therapeutic efficacy *in vitro* and *in vivo*. We propose that Ivermectin may be a good candidate for combination immunotherapy given its potential to synergize with clinically relevant PI3K/mTOR-inhibiting agents and its ability to modulate the P2X4/P2X7/Pannexin-1 pathway that appears to play a central role in both chemoresistance and ICD (Figure 7)

Plans for the next 12 months:

- Evaluate other potential Ivermectin-based synergistic drug combinations based on our preliminary *in vitro* studies, including Carfilzomib and other proteasome inhibitors.

- Evaluate the ability of Ivermectin to induce immunogenic cell death in the 4T1.2 triple-negative breast cancer model, alone or in combination with other drugs. Parallel studies will be performed in an Ova-expressing breast cancer model in order to study the effect of our drug combination on anti-tumor antigen-specific responses.

- Investigate the effect of adding PD-1 checkpoint blockade, with the hope that further potentiation of the anti-tumor immune responses induced by the combination of IVM and other drugs might result in durable and curative responses.

- Using an in vivo model, determine whether Ivermectin induces or inhibits tumor progression and whether the mechanism is through the immune response or other methods

Supporting Data/Figures:

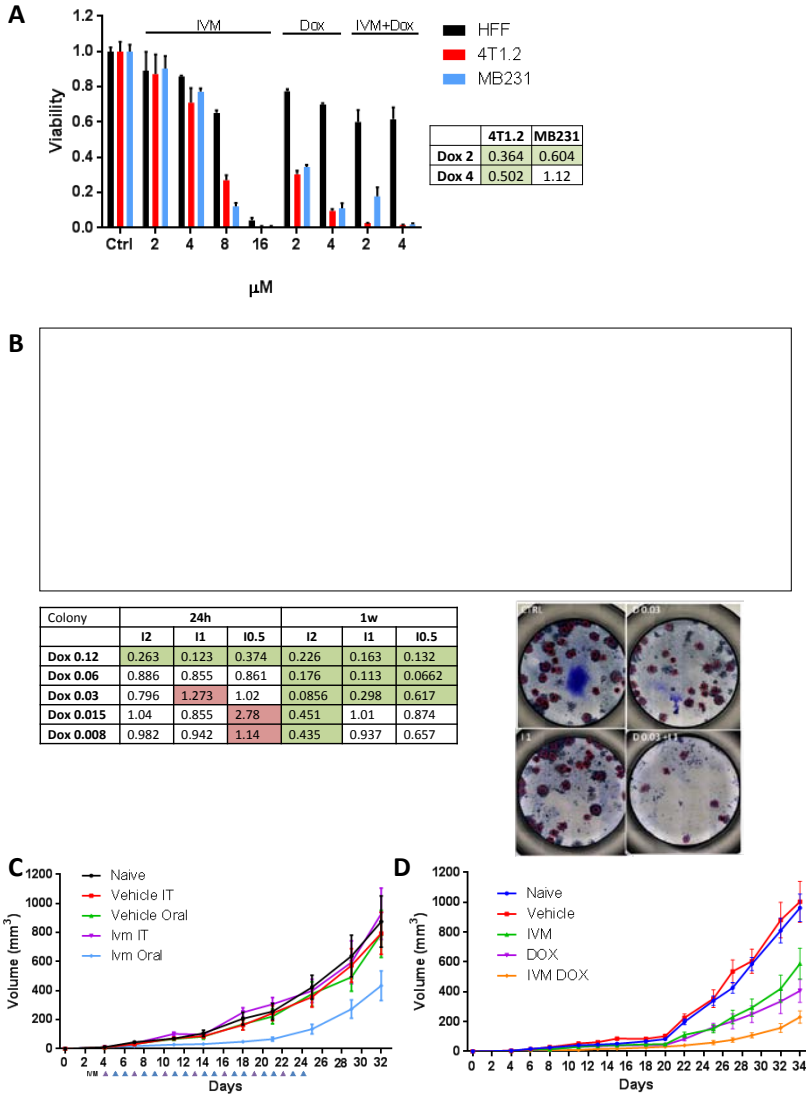

	4T1.2	MB231
Dox 2	0.364	0.604
Dox 4	0.502	1.12

Colony	24h			1w		
	I2	I1	I0.5	I2	I1	I0.5
Dox 0.12	0.263	0.123	0.374	0.226	0.163	0.132
Dox 0.06	0.886	0.855	0.861	0.176	0.113	0.0662
Dox 0.03	0.796	1.273	1.02	0.0856	0.298	0.617
Dox 0.015	1.04	0.855	2.78	0.451	1.01	0.874
Dox 0.008	0.982	0.942	1.14	0.435	0.937	0.657

Figure 1. Ivermectin-based synergistic combinations are effective against triple-negative breast cancer *in vitro* and *in vivo*.

(A) Ivermectin is synergistic with doxorubicin in the murine (4T1.2) and human (MDA-MB-231) TNBC cells. Cells were treated with Ivermectin alone, doxorubicin alone, or 4 µm of Ivermectin with the indicated concentration of doxorubicin. Combination Index (CI) values were evaluated with Calcusyn on cells used in a short 48h viability assay and values of less than 1 (green colored boxes) are indicative of synergy. (B) Physiological relevancy of the synergy between Ivermectin and doxorubicin was further validated with a one week colony assay on cells exposed to the lower doses of the drugs as indicated in the panels. 4T1.2 cells (100 cells per 96 well plate) were treated with Ivermectin and doxorubicin at the indicated concentrations for one week or drugs were washed away after the initial 24h. Colonies containing more than 50 cells were counted and data were normalized to untreated control cells. CI values indicating synergy/antagonism are shown in the accompanying table. Representative colonies treated with Ivermectin or doxorubicin alone or in combination are shown. (C) Balb/c mice were challenged with 4T1.2 cells orthotopically in the mammary gland and received 21 oral (OR) daily doses of Ivermectin (5 mg/kg) alone or in combination with doxorubicin at 5 mg/kg. A group of mice received their daily Ivermectin doses intratumorally instead of orally once every 3 days (IT). ($p=0.001$). (D) Balb/c mice were challenged with 4T1.2 cells orthotopically in the mammary gland and received 6 oral daily doses of Ivermectin (5 mg/kg) alone or in combination with doxorubicin at 5 mg/kg. Comparisons between doxorubicin or Ivermectin vs, doxorubicin + Ivermectin were $p \leq 0.05$. Data is representative of two independent experiments.

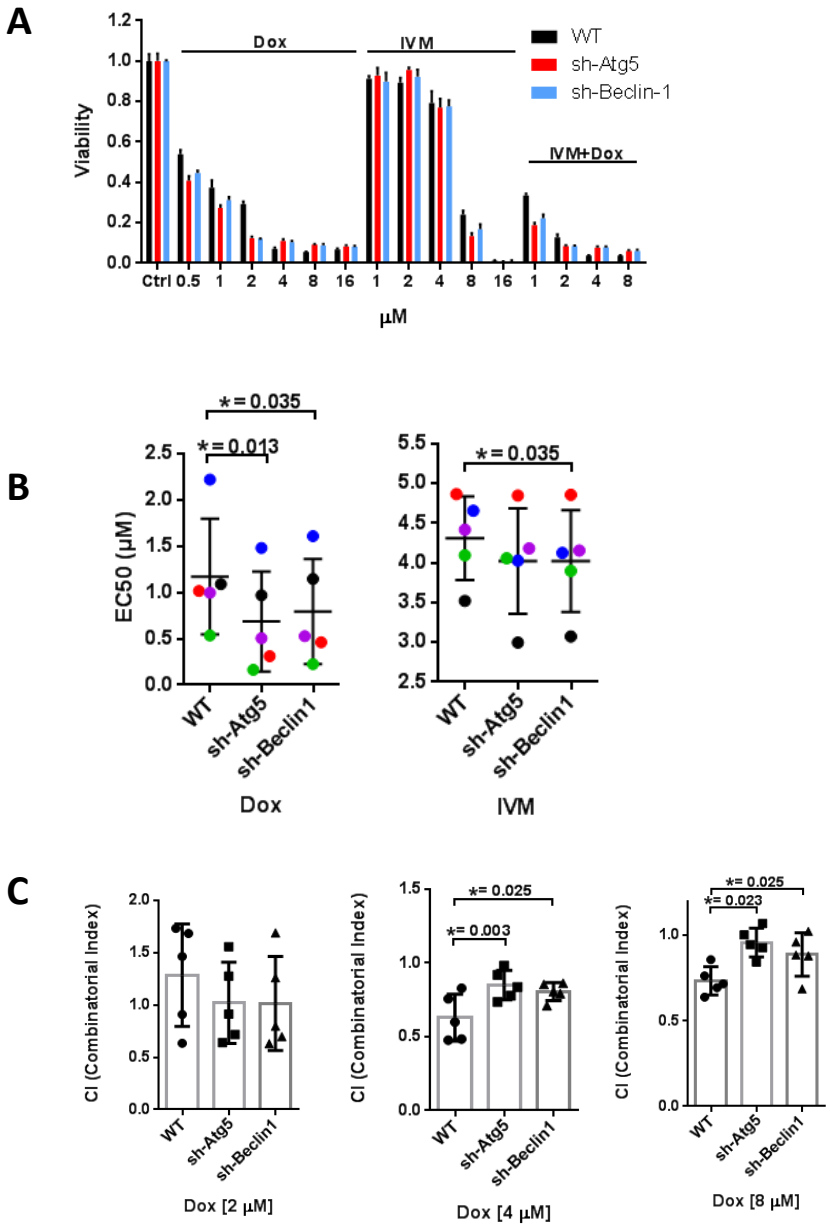

Figure 2. Synergy between doxorubicin and Ivermectin is dependent on autophagy.
(A) Synergy between doxorubicin and Ivermectin in autophagy deficient TNBC cells. Viability of wild type and shAtg5 or shBeclin-1 autophagy-deficient MDA-MB-231 cells treated with doxorubicin, Ivermectin, or doxorubicin and 4 µM Ivermectin for 48h. Shown is a representative experiment of 5 replicate experiments. (B) EC50 values showing the effect of autophagy deficiency on sensitivity to doxorubicin and Ivermectin. (C) Synergy requires doses of doxorubicin higher than the EC50 concentration and autophagy deficiency appears to interfere with the synergy between doxorubicin and Ivermectin.

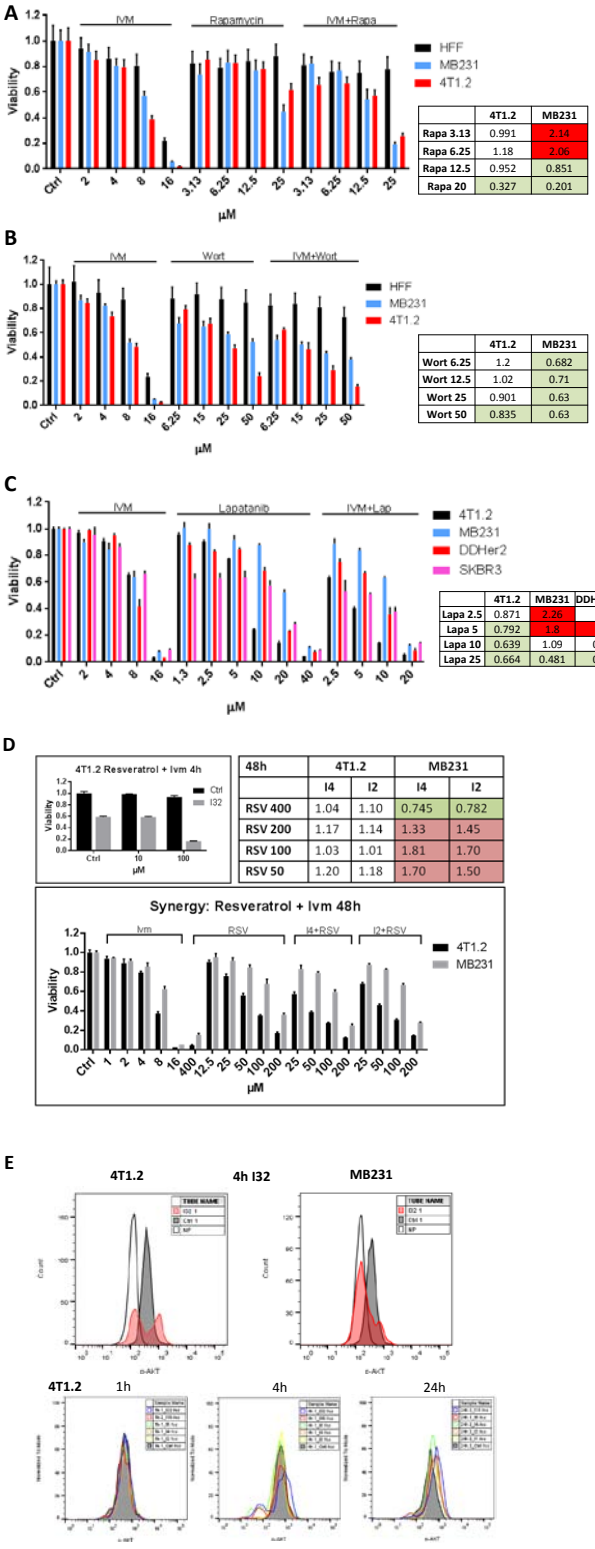

	4T1.2	MB231
Rapa 3.13	0.991	2.14
Rapa 6.25	1.18	2.06
Rapa 12.5	0.952	0.851
Rapa 20	0.327	0.201

	4T1.2	MB231
Wort 6.25	1.2	0.682
Wort 12.5	1.02	0.71
Wort 25	0.901	0.63
Wort 50	0.835	0.63

	4T1.2	MB231	DDHer2	SKBR3
Lapa 2.5	0.871	2.26	1.24	1.02
Lapa 5	0.792	1.8	1.43	1.45
Lapa 10	0.639	1.09	0.976	1.36
Lapa 25	0.664	0.481	0.479	0.617

48h	4T1.2		MB231	
	I4	I2	I4	I2
RSV 400	1.04	1.10	0.745	0.782
RSV 200	1.17	1.14	1.33	1.45
RSV 100	1.03	1.01	1.81	1.70
RSV 50	1.20	1.18	1.70	1.50

Figure 3. Ivermectin synergizes with a broad spectrum of autophagy-inducing therapeutics.
4T1.2 or MB231 cells were treated with Ivermectin alone or (A) Rapamycin, (B) Wortmannin, (C) Lapatinib, alone at the designated concentrations. To test for synergy cells were treated with a combination of 4 µM of Ivermectin and the respective drug at the designated concentrations as shown for 48 hours and percent viability was determined. The plots shown were normalized to untreated control for each cell type (control). Synergy (green) and antagonism (red) is shown with the corresponding CI values. Specificity for the clinically relevant therapeutics is shown by comparison with human foreskin fibroblasts (HFF) as normal un-transformed cells. As Lapatinib is a dual EGFR/Her-2 inhibitor, DDHer2 and SKBR3 cells were also included as murine and human

Her-2-positive control cells, respectively. (D) 4T1.2 and MB231 cells were treated with Ivermectin or Resveratrol alone or in combination at the indicated concentrations for 4 or 48 hours. (E) Cells were treated with Ivermectin at 2, 4, 8, 16, or 32 µM concentrations and phosphorylation of AKT was measured by flow cytometry. Of note, the direct cytotoxicity of high doses of Ivermectin is associated with eventual loss of pAKT in a subset of the cells.

A

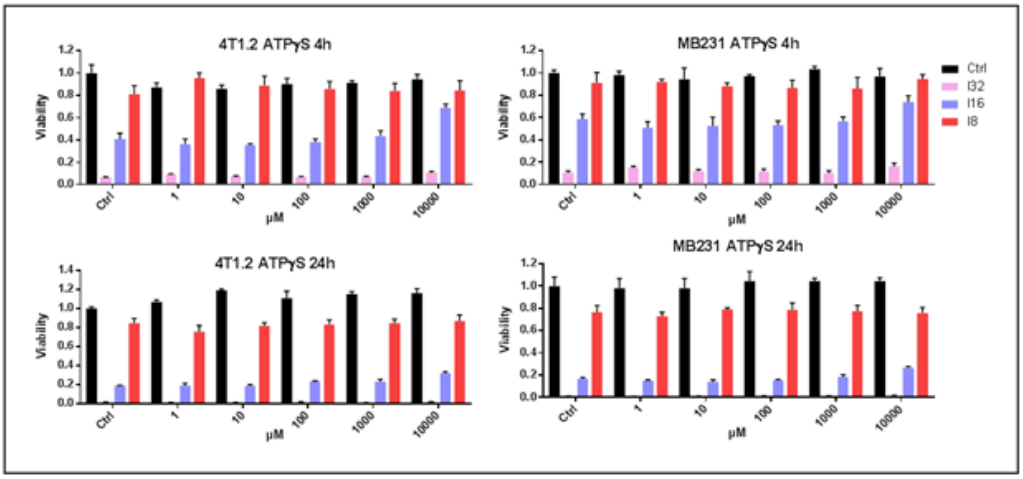

B

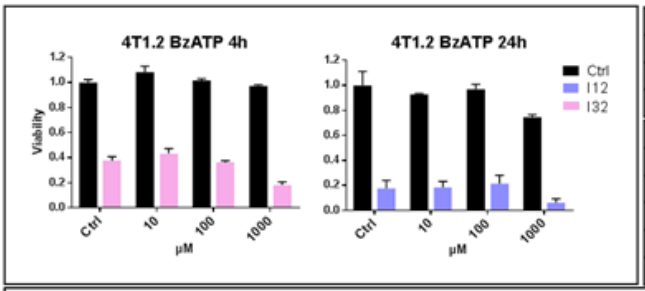

	I32/4h	I12/24h
Bz 1000	0.667	0.807
Bz 100	0.976	1.04
Bz 10	1.10	1.01

48h	4T1.2		MB231	
	I4	I2	I4	I2
LXR 50	0.316	0.568	0.783	0.958
LXR 25	1.18	1.25	0.816	0.983
LXR 12.5	1.49	1.43	1.09	1.22
LXR 6.25	1.45	1.37	1.06	0.618

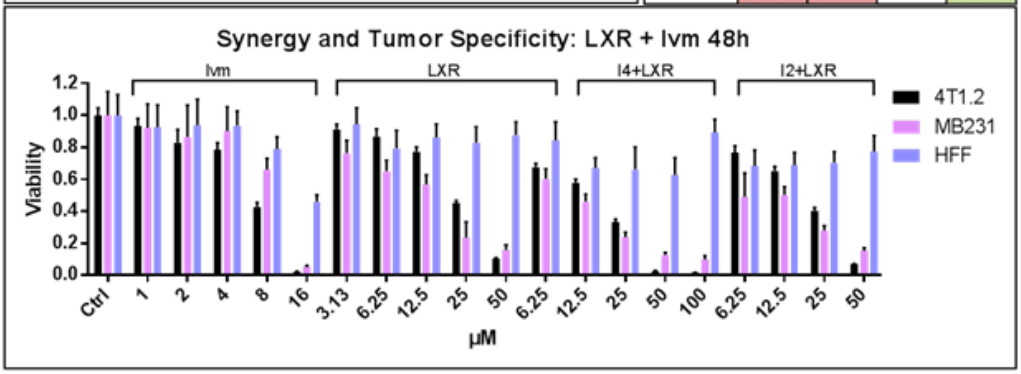

C

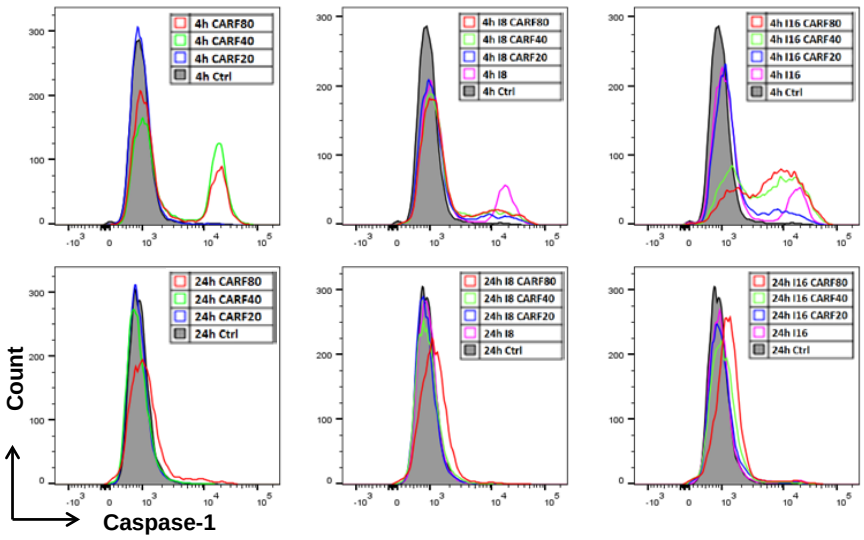

D

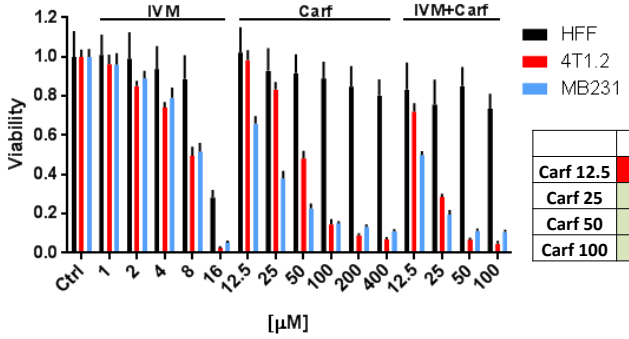

	4T1.2	MB231
Carf 12.5	1.3	1.22
Carf 25	0.523	0.412
Carf 50	0.292	0.314
Carf 100	0.393	0.482

E

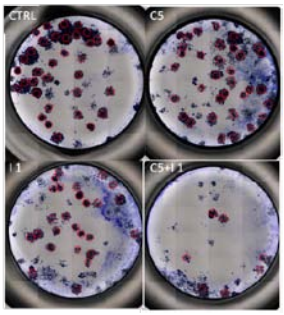

	24h Exposure			1W Exposure		
	I4	I2	I1	I4	I2	I1
Carf 20	0.413	0.346	0.316	NI	NI	NI
Carf 10	0.273	0.391	0.491	NI	0.597	0.358
Carf 5	0.574	1.16	0.938	NI	0.723	0.706
Carf 2.5	1.16	1.09	1.17	NI	0.943	0.880

Figure 4. Ivermectin is synergistic with other modulators of the P2X4/P2X7/Pannexin-1/NLRP3/Caspase-1 pathway.

(A) 4T1.2 cells were treated with a low affinity P2X7 agonist ATPγS (A) or high affinity P2X7 agonists BzATP or liver X receptor (LXR) (B) in combination with Ivermectin at the indicated concentrations and time points. (C) The proteasome inhibitor Carfilisomib induces massive activation of caspase-1 that can be further amplified by Ivermectin. Cells were treated with the indicated concentration of Carfilisomib for 4 or 24 hours. (D) Synergy between Carfilisomib and Ivermectin in murine and human TNBC cells. Cells were treated with Ivermectin alone, Carfilisomib alone, or 4 μM Ivermectin and Carfilisomib in combination. Synergistic values are indicated in green in the table. Tumor specificity is shown by comparison with human foreskin fibroblasts (HFF) as normal un-transformed cells. (E) A representative image of colonies treated with the respective drugs after one week of treatment with 5 μM Carfilisomib (C5) or 1 μM Ivermectin (I1) alone or in combination. CI values indicating synergy/antagonism are shown in the accompanying table.

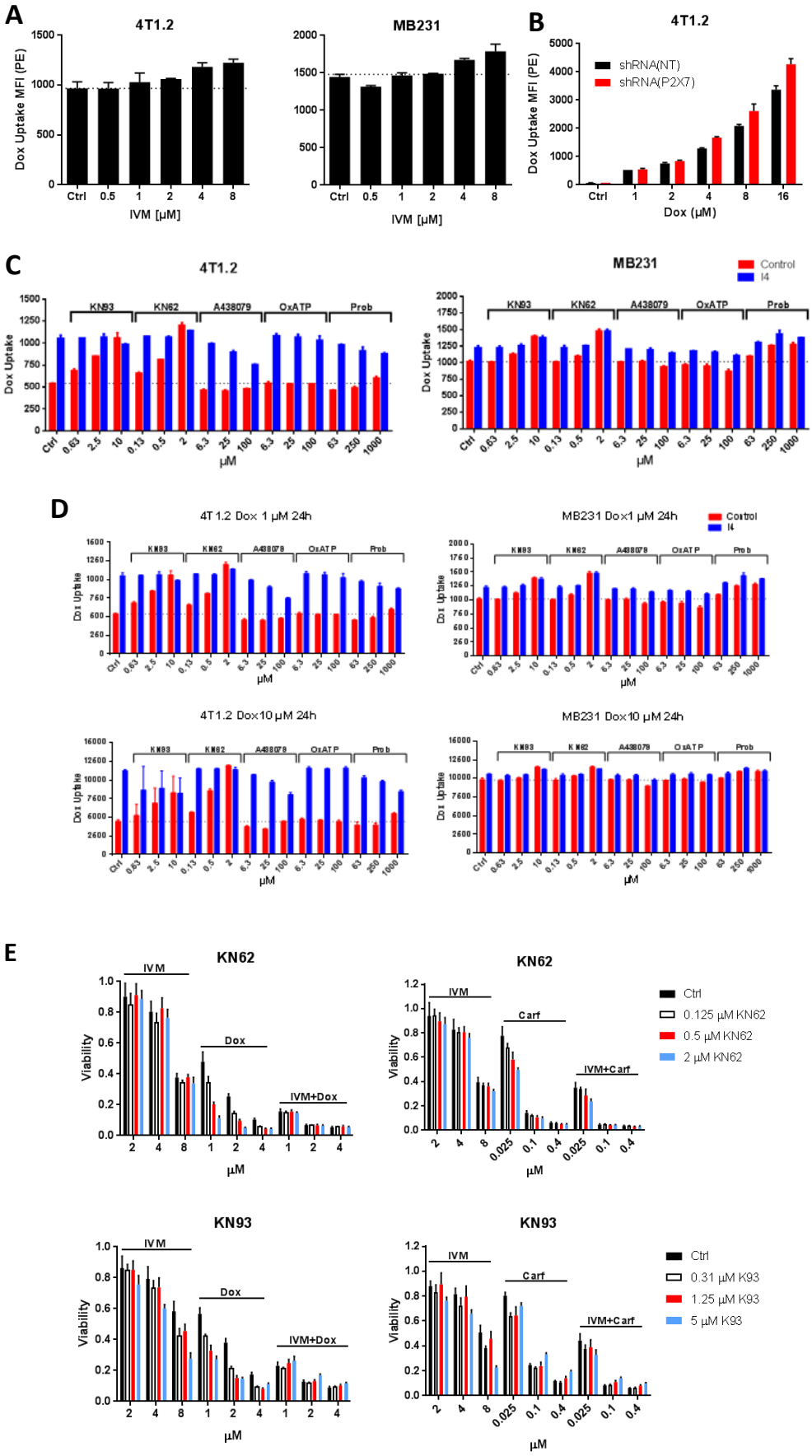
A
4T1.2
MB231
Dox Uptake MFI (PE)
IVM [μM]
Ctrl
0.5
1
2
4
8
B
4T1.2
shRNA(NT)
shRNA(P2X7)
Dox Uptake MFI (PE)
Dox (μM)
Ctrl
1
2
4
8
16
C
4T1.2
MB231
Control
I4
KN93
KN62
A438079
OxATP
Prob
Dox Uptake
μM
D
4T1.2 Dox 1 μM 24h
MB231 Dox1 μM 24h
4T1.2 Dox10 μM 24h
MB231 Dox10 μM 24h
E
KN62
KN93
IVM
Dox
IVM+Dox
Carf
IVM+Carf
Viability
μM
Ctrl
0.125 μM KN62
0.5 μM KN62
2 μM KN62
0.31 μM K93
1.25 μM K93
5 μM K93

Figure 5. Ivermectin compromises the protective functions of ATP release and purinergic signaling mediated by P2X7 receptors, Pannexin-1 channels and CAMKII.
(A) Ivermectin enhanced accumulation of doxorubicin in murine (4T1.2) and human (MDA-MB-231) triple-negative breast cancer cells. Tumor cells were treated with 1 μM doxorubicin in the presence of various doses of Ivermectin. Doxorubicin uptake was evaluated by flow cytometry. (B) P2X7-deficiency augments the accumulation of doxorubicin in 4T1.2 breast cancer cells. Control and P2X7-deficient 4T1.2 cells were treated with various doses of doxorubicin for 24h and analyzed as above. (C) Interference with the activity of the P2X4/P2X7/Pannexin-1 complex modulates the accumulation of doxorubicin. Murine and human breast cancer cells were treated with 1 μM doxorubicin for 24h in the presence of inhibitors of CaMKII (KN-93), the P2X7 receptor (KN-62, A438079, and oxATP) or the Pannexin-1 channel (Probenecid). (D) Interference with the activity of the P2X4/P2X7/Pannexin-1 complex modulates the accumulation of doxorubicin. Murine and human breast cancer cells were treated with 1 or 10 μM doxorubicin for 24h in the presence of inhibitors of CaMKII (KN-93), the P2X7 receptor (KN-62, A438079, and oxATP) or the Pannexin-1 channel (Probenecid). (E) Inhibition of P2X7 or CaMKII with lower non-toxic doses of KN62 and KN93, respectively, completely eliminates the synergy between doxorubicin and Ivermectin but only partly diminishes the synergy between Carfilisomib and Ivermectin. The murine 4T1.2 cells were treated with various combinations of Ivermectin, doxorubicin, Carfilisomib and P2X7/CaMKII inhibitors for 48h at the indicated concentrations.

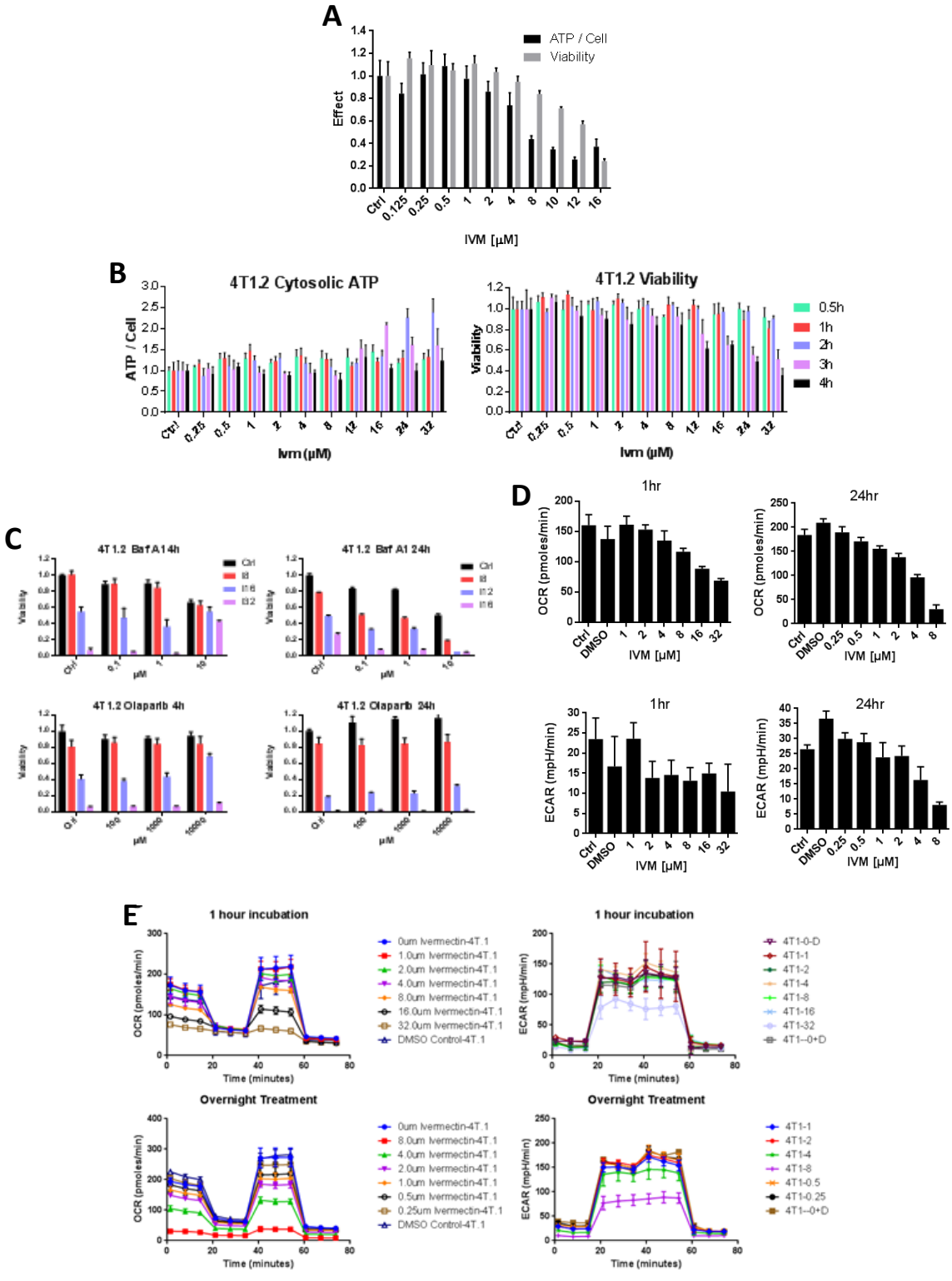
A
ATP / Cell
Viability
Effect
IVM [µM]
B
4T1.2 Cytosolic ATP
ATP / Cell
Ivm (µM)
4T1.2 Viability
Viability
0.5h
1h
2h
3h
4h
C
4T1.2 Baf A1 4h
4T1.2 Baf A1 24h
4T1.2 Olaparib 4h
4T1.2 Olaparib 24h
D
1hr
24hr
OCR (pmoles/min)
ECAR (mpH/min)
IVM [µM]
E
1 hour incubation
Overnight Treatment
Time (minutes)
0um Ivermectin-4T.1
1.0um Ivermectin-4T.1
2.0um Ivermectin-4T.1
4.0um Ivermectin-4T.1
8.0um Ivermectin-4T.1
16.0um Ivermectin-4T.1
32.0um Ivermectin-4T.1
DMSO Control-4T.1
0.5um Ivermectin-4T.1
0.25um Ivermectin-4T.1
4T1-0-D
4T1-1
4T1-2
4T1-4
4T1-8
4T1-16
4T1-32
4T1--0+D
4T1-0.5
4T1-0.25

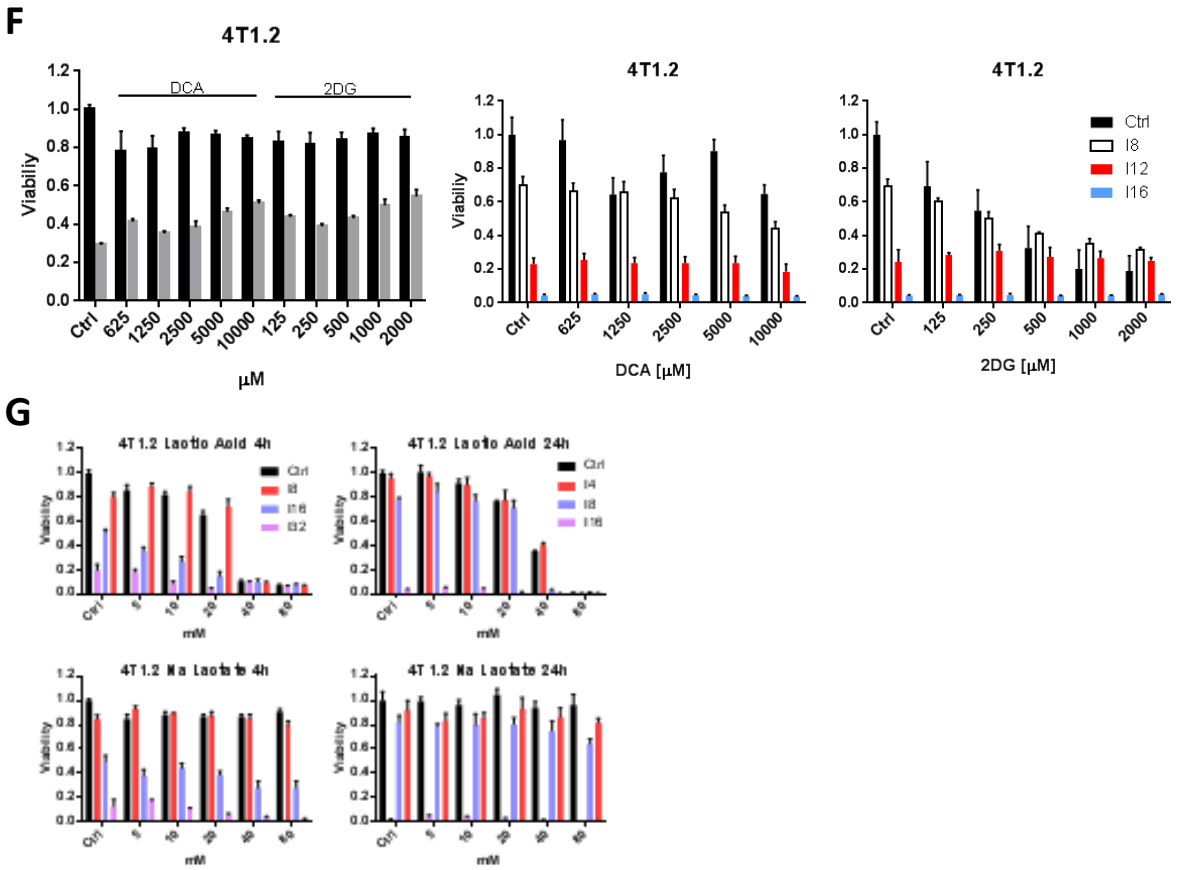

Figure 6. Ivermectin compromises cellular ATP metabolism.
(A) Ivemectin induces a dose-dependent depletion of cellular ATP reserves. 4T1.2 cells engineered to express cytosolic Luciferase were exposed to different doses of Ivemectin for 24h and cytosolic ATP levels were evaluated by Luciferin luminescence and normalized to cell viability. (B) Ivermectin induced a transient increase in cytosolic ATP. 4T1.2 cells engineered to express cytosolic Luciferase were exposed to different doses of Ivemectin for 0.5h-4h and cytosolic ATP levels were evaluated by Luciferin luminescence and normalized to cell viability. (C) Inhibition of vacuolar type H+- ATPase or PARP by Bafilomycin A and Olaparib, respectively, provides partial protection against acute doses of Ivermectin in murine and human TNBC cells. (D) Ivermectin preferentially inhibits mitochondrial respiration over glycolysis. 4T1.2 cell were pretreated with different doses of Ivermectin for 1h or 24h prior to Seahorse analysis. The plots show the effect of Ivermectin on the basal levels of mitochondrial respiration (left two panels) and glycolysis (right two panels), respectively. (E) Ivermectin inhibits mitochondrial respiration while having minimal immediate effects on glycolysis. 4T1.2 cell were pretreated with different doses of Ivermectin for 1h 24h prior to Seahorse analysis. Raw data plots are shown. (F) Murine 4T1.2 cells were treated with media (black) or 32 µM of Ivermectin (grey) for 4h in the presence of DCA or 2DG at the indicated concentrations (left). 4T1.2 cells were treated with 8 µM, 12 µM, or 16 µM of Ivermectin for 24h with the indicated concentrations of DCA or 2DG (middle and right panels). (G) Lactic acid but not sodium lactate exacerbates Ivermectin cytotoxicity in both murine and human TNBC cells.

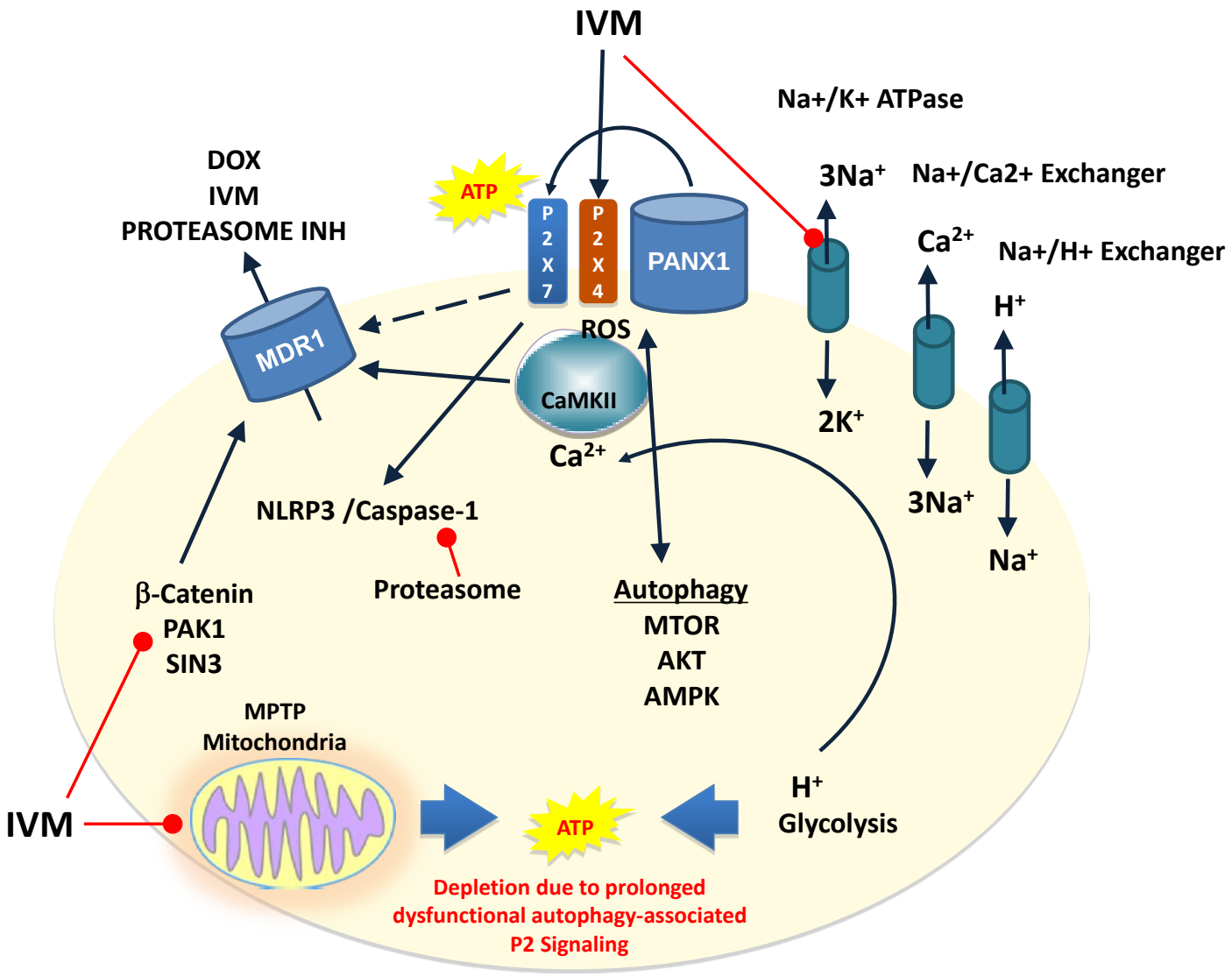

Figure 7. Ivermectin synergizes with autophagy inducing drugs by compromising the protective functions of purinergic signaling mediated by the P2X4/P2X7/Pannexin-1 complex.
Ivermectin induces autophagy and potentiates P2X4/P2X7/Pannexin-1 signaling that normally mediates defensive functions such as up-regulation or activation of MDR1, which exports cytotoxic drugs such as doxorubicin, proteasome inhibitors, and others, including Ivermectin itself. In addition to being a direct substrate and competitive inhibitor of the MDR1 pump, Ivermectin has also been shown to directly or indirectly target the Na+/K+ ATPase, b-catenin, PAK1 and SIN3, pathways that have also been implicated in the regulation of MDR1 activity, thus explaining why MDR1 functions can be compromised despite its elevated surface expression levels. Paradoxically, Ivermectin potentiates a defensive purinergic signaling pathway but appears synergistic with cytotoxic drugs. We have shown that Ivermectin inhibits mitochondrial respiration and glycolysis appears insufficient to compensate the depletion of cellular ATP due to acidification and compensatory increase in cytosolic Ca2+. Thus Ivermectin potentiates defensive P2X4/P2X7/Pannexin-1 signaling only transiently, and alone or in combination with other autophagy- inducing drugs can compromise the defensive purinergic signaling and be broadly synergistic. This might involve a complex interplay between competitive inhibition of the MDR1 pump coupled to compensatory, exaggerated, and dysfunctional purinergic signaling.

KEY RESEARCH ACCOMPLISHMENTS:

- Determined that cancer-associated fibroblasts (CAFs) derived from human breast cancer brain metastases express significantly higher levels of CXCL12 and CXCL16 than fibroblasts from primary breast tumors and normal breast.

- 3-D CAF aggregates from brain metastasis promote cancer cell migration more effectively than CAF aggregates derived from primary tumor or normal breast stromal cells.

- Treatment with a CXCR4 antagonist and/or CXCL16 neutralizing antibody, alone or in combination significantly inhibited migration of cancer cells to brain metastatic CAF aggregates.

- Established that dysfunctional IL-6 signaling responses in CD4+ naïve T cells from breast cancer patients are caused by reduced expression in both chains of the IL-6 receptor through two distinct mechanisms: a) reduced transcriptional levels of gp130 and, b) enhanced cleavage of the IL-6Rα chain by ADAM17.
- IL-27, which shares the common gp130 receptor as IL-6, signaling responses in CD4 naïve T cells were also blunted in breast cancer patient's vs healthy controls. However, the defects in signaling were not found to be correlated with clinical outcome.

- Generated data which suggests that IL-6 signaling responsiveness in peripheral $CD4^+$ naïve T cells could be used to predict the clinical outcome of breast cancer patients.

- Determined that IL-10 signaling responses in breast cancer patient CD8 T cells were significantly higher than healthy donor CD8 T cells. However, the enhanced signaling responses in breast cancer patient CD8 T cells was not correlated with clinical outcome.

- Found blunted IFNγ signaling in CD33+ myeloid cells of breast cancer patients compared to healthy donors and that lower IFNγ signaling responses in CD33+ myeloid cells may predict worse relapse-free survival.

- Showed that Ivermectin-mediated modulation of purinergic signaling can impact the balance of autophagy-dependent pro-survival and cytotoxic signals, sensitizing breast cancer cells to a broad spectrum of autophagy-inducing therapeutics.

- Demonstrated that Ivermectin is synergistic with a broad spectrum of clinically relevant autophagy inducing therapeutics and that some of these synergies are tumor-specific which can be validated in vivo.

- Established that synergy was dependent on autophagy and correlated with depletion of ATP cellular reserves and interference with the normally protective functions of purinergic signaling in cancer mediated by P2X7 receptors, Pannexin-1 channels and CAMKII.

.

REPORTABLE OUTCOMES: Provide a list of reportable outcomes that have resulted from this research to include:

- Ivermectin synergizes with autophagy inducing drugs by compromising protective P2X4/P2X7/Pannexin-1 signaling in cancer cells. Manuscript in preparation
- Chung B, Esmaeili A, Murad JP, Andersen E, et al. Human brain metastatic stroma recruits breast cancer cells via chemokines CXCL16 and CXCL12. NPJ Breast Cancer, in press.
- Wang L, Miyahira AK, Simons DL, Lu X, Chang A, Suni M, Maino VC, Dirbas FM, Yim JH, Waisman J, Lee PP. IL-6 Signaling in Peripheral Blood T cells Predicts Clinical Outcome in Breast Cancer. Cancer Res. 2016 Nov 22. e1373

CONCLUSION:

We have a strong research team for this project, which includes assistant research professor Dr. Brile Chung, staff scientist Dr. Young Min Chung, PhD postdoctoral fellow Dr. Manasi Kamat, and research associate Gilbert Acosta. We have worked closely with the CoH IACUC office on animal protocols and two have been approved. We continue to develop an in-depth understanding of the immune system within the setting of the tumor microenvironment. We have made progress in developing methods to better analyze the relationships between primary tumor and metastatic growths with their surrounding microenvironment and implications for immune response and dendritic cell function *in vitro* using 3D microculture techniques. We have further investigated and tested alternative methods of combinatorial drugs in attempts to eradicate cancer cells while preserving the immune system. We are well positioned to gain further insights in the next 12 months that will aid in our goal of restoring long term immune function in breast cancer patients to optimal levels, and subsequently eradicate metastases to prevent relapse in breast cancer patients.

APPENDICES:

None at this time.

PERSONNEL:

Peter P. Lee, MD – PI	25% Effort
Brile Chung, PhD – Assistant Research Professor	100% Effort
Young Min Chung, PhD – Staff Scientist	60% Effort
Manasi Kamat, PhD – Post Doctoral Fellow	100% Effort
Gilbert Acosta, Research Associate I	50% Effort

REFERENCES:

1. E. Adinolfi *et al.*, Expression of P2X7 receptor increases in vivo tumor growth. *Cancer research* **72**, 2957 (Jun 15, 2012).
2. C. N. Baxevanis *et al.*, Tumor specific cytolysis by tumor infiltrating lymphocytes in breast cancer. *Cancer* **74**, 1275 (Aug 15, 1994).
3. G. B. Cannon, R. Pomerantz, Cell-mediated immune responses--prognostic indicators of survival from breast cancer. *Int J Cancer* **44**, 995 (Dec 15, 1989).
4. J. L. McCoy, R. Rucker, J. A. Petros, Cell-mediated immunity to tumor-associated antigens is a better predictor of survival in early stage breast cancer than stage, grade or lymph node status. *Breast cancer research and treatment* **60**, 227 (Apr, 2000).
5. H. E. Kohrt *et al.*, Profile of immune cells in axillary lymph nodes predicts disease-free survival in breast cancer. *PLoS Med* **2**, e284 (Sep, 2005).
6. B. Weigelt, A. T. Lo, C. C. Park, J. W. Gray, M. J. Bissell, HER2 signaling pathway activation and response of breast cancer cells to HER2-targeting agents is dependent strongly on the 3D microenvironment. *Breast cancer research and treatment* **122**, 35 (Jul, 2010).
7. M. Batten *et al.*, Interleukin 27 limits autoimmune encephalomyelitis by suppressing the development of interleukin 17-producing T cells. *Nature immunology* **7**, 929 (Sep, 2006).
8. M. Vanneman, G. Dranoff, Combining immunotherapy and targeted therapies in cancer treatment. *Nature reviews. Cancer* **12**, 237 (Apr, 2012).
9. B. Ljujic *et al.*, Human mesenchymal stem cells creating an immunosuppressive environment and promote breast cancer in mice. *Scientific reports* **3**, 2298 (Jul 29, 2013).
10. T. D. Tlsty, L. M. Coussens, Tumor stroma and regulation of cancer development. *Annual review of pathology* **1**, 119 (2006).
11. M. M. Shao *et al.*, A subset of breast cancer predisposes to brain metastasis. *Medical molecular morphology* **44**, 15 (Mar, 2011).
12. K. D. Miller *et al.*, Occult central nervous system involvement in patients with metastatic breast cancer: prevalence, predictive factors and impact on overall survival. *Annals of oncology : official journal of the European Society for Medical Oncology / ESMO* **14**, 1072 (Jul, 2003).
13. I. J. Fidler, S. Yano, R. D. Zhang, T. Fujimaki, C. D. Bucana, The seed and soil hypothesis: vascularisation and brain metastases. *The Lancet. Oncology* **3**, 53 (Jan, 2002).
14. A. J. Minn *et al.*, Distinct organ-specific metastatic potential of individual breast cancer cells and primary tumors. *The Journal of clinical investigation* **115**, 44 (Jan, 2005).
15. M. Majety, L. P. Pradel, M. Gies, C. H. Ries, Fibroblasts Influence Survival and Therapeutic Response in a 3D Co-Culture Model. *PLoS One* **10**, e0127948 (2015).
16. B. Chung *et al.*, Engineering the human thymic microenvironment to support thymopoiesis in vivo. *Stem cells* **32**, 2386 (Sep, 2014).
17. P. Sethi *et al.*, 3D tumor tissue analogs and their orthotopic implants for understanding tumor-targeting of microenvironment-responsive nanosized chemotherapy and radiation. *Nanomedicine : nanotechnology, biology, and medicine* **11**, 2013 (Nov, 2015).
18. O. S. Aljitawi *et al.*, A novel three-dimensional stromal-based model for in vitro chemotherapy sensitivity testing of leukemia cells. *Leukemia & lymphoma* **55**, 378 (Feb, 2014).
19. A. Muller *et al.*, Involvement of chemokine receptors in breast cancer metastasis. *Nature* **410**, 50 (Mar 1, 2001).
20. F. J. Lv, R. S. Tuan, K. M. Cheung, V. Y. Leung, Concise review: the surface markers and identity of human mesenchymal stem cells. *Stem cells* **32**, 1408 (Jun, 2014).
21. P. J. Psaltis *et al.*, Enrichment for STRO-1 expression enhances the cardiovascular paracrine activity of human bone marrow-derived mesenchymal cell populations. *Journal of cellular physiology* **223**, 530 (May, 2010).
22. E. R. Shamir, A. J. Ewald, Three-dimensional organotypic culture: experimental models of mammalian biology and disease. *Nature reviews. Molecular cell biology* **15**, 647 (Oct, 2014).

23. A. Desmouliere, C. Chaponnier, G. Gabbiani, Tissue repair, contraction, and the myofibroblast. *Wound repair and regeneration : official publication of the Wound Healing Society [and] the European Tissue Repair Society* **13**, 7 (Jan-Feb, 2005).
24. Y. Mao, Keller, E.T., Garfield, D.H., Shen, K. & Wang, J., Stromal cells in tumor microenvironment and breast cancer. *Cancer Metastasis Rev*, 303 (2012).
25. M. Yamashita *et al.*, Role of stromal myofibroblasts in invasive breast cancer: stromal expression of alpha-smooth muscle actin correlates with worse clinical outcome. *Breast cancer* **19**, 170 (Apr, 2012).
26. H. I. Kornblum, D. H. Geschwind, Molecular markers in CNS stem cell research: hitting a moving target. *Nature reviews. Neuroscience* **2**, 843 (Nov, 2001).
27. H. Kang *et al.*, Stromal cell derived factor-1: its influence on invasiveness and migration of breast cancer cells in vitro, and its association with prognosis and survival in human breast cancer. *Breast cancer research : BCR* **7**, R402 (2005).
28. P. J. Sarvaiya, D. Guo, I. Ulasov, P. Gabikian, M. S. Lesniak, Chemokines in tumor progression and metastasis. *Oncotarget* **4**, 2171 (Dec, 2013).
29. M. Matloubian, A. David, S. Engel, J. E. Ryan, J. G. Cyster, A transmembrane CXC chemokine is a ligand for HIV-coreceptor Bonzo. *Nature immunology* **1**, 298 (Oct, 2000).
30. Y. Lu *et al.*, CXCL16 functions as a novel chemotactic factor for prostate cancer cells in vitro. *Molecular cancer research : MCR* **6**, 546 (Apr, 2008).
31. L. Deng, N. Chen, Y. Li, H. Zheng, Q. Lei, CXCR6/CXCL16 functions as a regulator in metastasis and progression of cancer. *Biochimica et biophysica acta* **1806**, 42 (Aug, 2010).
32. P. M. Hershberger *et al.*, in *Probe Reports from the NIH Molecular Libraries Program*. (Bethesda (MD), 2010).
33. N. S. Zuckerman, Y. Noam, A. J. Goldsmith, P. P. Lee, A self-directed method for cell-type identification and separation of gene expression microarrays. *PLoS computational biology* **9**, e1003189 (Aug, 2013).
34. M. Kopf *et al.*, Impaired immune and acute-phase responses in interleukin-6-deficient mice. *Nature* **368**, 339 (Mar 24, 1994).
35. P. C. Heinrich, I. Behrmann, G. Muller-Newen, F. Schaper, L. Graeve, Interleukin-6-type cytokine signalling through the gp130/Jak/STAT pathway. *The Biochemical journal* **334 (Pt 2)**, 297 (Sep 1, 1998).
36. H. Korkaya, S. Liu, M. S. Wicha, Regulation of Cancer Stem Cells by Cytokine Networks: Attacking Cancers Inflammatory Roots. *Clin Cancer Res*, (Jun 17, 2011).
37. H. Knupfer, R. Preiss, Significance of interleukin-6 (IL-6) in breast cancer (review). *Breast cancer research and treatment* **102**, 129 (Apr, 2007).
38. R. Salgado *et al.*, Circulating interleukin-6 predicts survival in patients with metastatic breast cancer. *Int J Cancer* **103**, 642 (Feb 20, 2003).
39. A. Kimura, T. Kishimoto, IL-6: regulator of Treg/Th17 balance. *European journal of immunology* **40**, 1830 (Jul, 2010).
40. X. Zhang, T. Goel, L. L. Goodfield, S. J. Muse, E. T. Harvill, Decreased leukocyte accumulation and delayed Bordetella pertussis clearance in IL-6-/- mice. *J Immunol* **186**, 4895 (Apr 15, 2011).
41. S. Pflanz *et al.*, WSX-1 and glycoprotein 130 constitute a signal-transducing receptor for IL-27. *J Immunol* **172**, 2225 (Feb 15, 2004).
42. E. Tassi *et al.*, Non-redundant role for IL-12 and IL-27 in modulating Th2 polarization of carcinoembryonic antigen specific CD4 T cells from pancreatic cancer patients. *PLoS One* **4**, e7234 (2009).
43. T. Yoshimoto, K. Yasuda, J. Mizuguchi, K. Nakanishi, IL-27 suppresses Th2 cell development and Th2 cytokines production from polarized Th2 cells: a novel therapeutic way for Th2-mediated allergic inflammation. *J Immunol* **179**, 4415 (Oct 1, 2007).
44. S. Pflanz *et al.*, IL-27, a heterodimeric cytokine composed of EBI3 and p28 protein, induces proliferation of naive CD4(+) T cells. *Immunity* **16**, 779 (Jun, 2002).
45. N. Morishima *et al.*, A pivotal role for interleukin-27 in CD8+ T cell functions and generation of cytotoxic T lymphocytes. *J Biomed Biotechnol* **2010**, 605483 (2010).

46. N. Morishima *et al.*, Augmentation of effector CD8+ T cell generation with enhanced granzyme B expression by IL-27. *J Immunol* **175**, 1686 (Aug 1, 2005).
47. K. P. Strauss, Implementing the telecommunications provisions. *Milbank Q* **69 Suppl 1-2**, 238 (1991).
48. G. Regis, S. Pensa, D. Boselli, F. Novelli, V. Poli, Ups and downs: the STAT1:STAT3 seesaw of Interferon and gp130 receptor signalling. *Semin Cell Dev Biol* **19**, 351 (Aug, 2008).
49. L. Y. Kong *et al.*, A novel phosphorylated STAT3 inhibitor enhances T cell cytotoxicity against melanoma through inhibition of regulatory T cells. *Cancer Immunol Immunother* **58**, 1023 (Jul, 2009).
50. M. Kortylewski *et al.*, Inhibiting Stat3 signaling in the hematopoietic system elicits multicomponent antitumor immunity. *Nat Med* **11**, 1314 (Dec, 2005).
51. C. Dethlefsen, G. Hojfeldt, P. Hojman, The role of intratumoral and systemic IL-6 in breast cancer. *Breast cancer research and treatment* **138**, 657 (Apr, 2013).
52. Q. Chang *et al.*, The IL-6/JAK/Stat3 feed-forward loop drives tumorigenesis and metastasis. *Neoplasia* **15**, 848 (Jul, 2013).
53. X. J. Wang *et al.*, gp130, the cytokine common signal-transducer of interleukin-6 cytokine family, is downregulated in T cells in vivo by interleukin-6. *Blood* **91**, 3308 (May 1, 1998).
54. E. Hidalgo *et al.*, The response of T cells to interleukin-6 is differentially regulated by the microenvironment of the rheumatoid synovial fluid and tissue. *Arthritis and rheumatism* **63**, 3284 (Nov, 2011).
55. H. H. Oberg, D. Wesch, S. Grussel, S. Rose-John, D. Kabelitz, Differential expression of CD126 and CD130 mediates different STAT-3 phosphorylation in CD4+CD25- and CD25high regulatory T cells. *International immunology* **18**, 555 (Apr, 2006).
56. N. Schumacher *et al.*, Shedding of Endogenous Interleukin-6 Receptor (IL-6R) Is Governed by A Disintegrin and Metalloproteinase (ADAM) Proteases while a Full-length IL-6R Isoform Localizes to Circulating Microvesicles. *J Biol Chem* **290**, 26059 (Oct 23, 2015).
57. O. Dienz, M. Rincon, The effects of IL-6 on CD4 T cell responses. *Clinical immunology* **130**, 27 (Jan, 2009).
58. J. S. Silver, C. A. Hunter, gp130 at the nexus of inflammation, autoimmunity, and cancer. *Journal of leukocyte biology* **88**, 1145 (Dec, 2010).
59. S. R. Bailey *et al.*, Th17 cells in cancer: the ultimate identity crisis. *Frontiers in immunology* **5**, 276 (2014).
60. I. Kryczek *et al.*, Phenotype, distribution, generation, and functional and clinical relevance of Th17 cells in the human tumor environments. *Blood* **114**, 1141 (Aug 6, 2009).
61. W. Zou, N. P. Restifo, T(H)17 cells in tumour immunity and immunotherapy. *Nature reviews. Immunology* **10**, 248 (Apr, 2010).
62. G. Murugaiyan, B. Saha, IL-27 in tumor immunity and immunotherapy. *Trends in molecular medicine* **19**, 108 (Feb, 2013).
63. S. Kamiya *et al.*, An indispensable role for STAT1 in IL-27-induced T-bet expression but not proliferation of naive CD4+ T cells. *J Immunol* **173**, 3871 (Sep 15, 2004).
64. T. Owaki *et al.*, STAT3 is indispensable to IL-27-mediated cell proliferation but not to IL-27-induced Th1 differentiation and suppression of proinflammatory cytokine production. *J Immunol* **180**, 2903 (Mar 1, 2008).
65. J. S. Stumhofer *et al.*, Interleukin 27 negatively regulates the development of interleukin 17-producing T helper cells during chronic inflammation of the central nervous system. *Nature immunology* **7**, 937 (Sep, 2006).
66. T. Yoshimoto, T. Yoshimoto, K. Yasuda, J. Mizuguchi, K. Nakanishi, IL-27 suppresses Th2 cell development and Th2 cytokines production from polarized Th2 cells: a novel therapeutic way for Th2-mediated allergic inflammation. *J Immunol* **179**, 4415 (Oct 1, 2007).
67. C. A. Hunter, R. Kastelein, Interleukin-27: balancing protective and pathological immunity. *Immunity* **37**, 960 (Dec 14, 2012).
68. Hamidullah, B. Changkija, R. Konwar, Role of interleukin-10 in breast cancer. *Breast cancer research and treatment* **133**, 11 (May, 2012).

69. R. J. Critchley-Thorne *et al.*, Impaired interferon signaling is a common immune defect in human cancer. *Proceedings of the National Academy of Sciences of the United States of America* **106**, 9010 (Jun 2, 2009).
70. L. Anasagasti-Angulo, Y. Garcia-Vega, S. Barcelona-Perez, P. Lopez-Saura, I. Bello-Rivero, Treatment of advanced, recurrent, resistant to previous treatments basal and squamous cell skin carcinomas with a synergistic formulation of interferons. Open, prospective study. *BMC Cancer* **9**, 262 (2009).
71. G. Kroemer, L. Galluzzi, O. Kepp, L. Zitvogel, Immunogenic cell death in cancer therapy. *Annual review of immunology* **31**, 51 (2013).
72. M. Michaud *et al.*, Autophagy-dependent anticancer immune responses induced by chemotherapeutic agents in mice. *Science* **334**, 1573 (Dec 16, 2011).
73. L. Menger *et al.*, Cardiac glycosides exert anticancer effects by inducing immunogenic cell death. *Science translational medicine* **4**, 143ra99 (Jul 18, 2012).
74. J. Pol *et al.*, Trial Watch: Immunogenic cell death inducers for anticancer chemotherapy. *Oncoimmunology* **4**, e1008866 (Apr, 2015).
75. A. Kawano *et al.*, Regulation of P2X7-dependent inflammatory functions by P2X4 receptor in mouse macrophages. *Biochemical and biophysical research communications* **420**, 102 (Mar 30, 2012).
76. J. K. Sandilos, D. A. Bayliss, Physiological mechanisms for the modulation of pannexin 1 channel activity. *The Journal of physiology* **590**, 6257 (Dec 15, 2012).
77. A. Boyd-Tressler, S. Penuela, D. W. Laird, G. R. Dubyak, Chemotherapeutic drugs induce ATP release via caspase-gated pannexin-1 channels and a caspase/pannexin-1-independent mechanism. *J Biol Chem* **289**, 27246 (Sep 26, 2014).
78. G. Burnstock, A. Verkhratsky, Long-term (trophic) purinergic signalling: purinoceptors control cell proliferation, differentiation and death. *Cell death & disease* **1**, e9 (2010).
79. A. Uspenskaia Iu *et al.*, [Features of expression and functional activity of P2X7 receptors in bone marrow cells under the action of doxorubicin]. *Eksperimental'naia i klinicheskaia farmakologiia* **70**, 52 (Jan-Feb, 2007).
80. D. Draganov *et al.*, Modulation of P2X4/P2X7/Pannexin-1 sensitivity to extracellular ATP via Ivermectin induces a non-apoptotic and inflammatory form of cancer cell death. *Scientific reports* **5**, 16222 (2015).
81. Y. Ma, L. Galluzzi, L. Zitvogel, G. Kroemer, Autophagy and cellular immune responses. *Immunity* **39**, 211 (Aug 22, 2013).
82. V. Vingtdeux *et al.*, AMP-activated protein kinase signaling activation by resveratrol modulates amyloid-beta peptide metabolism. *J Biol Chem* **285**, 9100 (Mar 19, 2010).
83. V. Derangere *et al.*, Liver X receptor beta activation induces pyroptosis of human and murine colon cancer cells. *Cell death and differentiation* **21**, 1914 (Dec, 2014).
84. S. Furusawa *et al.*, Potentiation of Doxorubicin-Induced Apoptosis of Resistant Mouse Leukaemia Cells by Ivermectin. *Pharmacy and Pharmacology Communications* **6**, 129 (2000).
85. Y. N. Korystov *et al.*, Avermectins inhibit multidrug resistance of tumor cells. *European journal of pharmacology* **493**, 57 (Jun 16, 2004).
86. N. H. Obata *et al.*, Effect of KN-62, Ca2+/calmodulin-dependent protein kinase II inhibitor, on adriamycin resistance of human ovarian cancer cells. *Biochemical and biophysical research communications* **215**, 566 (Oct 13, 1995).
87. S. J. Reshkin, R. A. Cardone, S. Harguindey, Na+-H+ exchanger, pH regulation and cancer. *Recent patents on anti-cancer drug discovery* **8**, 85 (Jan 1, 2013).